GEOSPHERE

GEOSPHERE, v. 17

https://doi.org/10.1130/GES02360.1

11 figures

CORRESPONDENCE: jsleeper@hawaii.edu

CITATION: Sleeper, J.D., Martinez, F., Fryer, P., Stern, R.J., Kelley, K.A., and Ohara, Y., 2021, Diffuse spreading, a newly recognized mode of crustal accretion in the southern Mariana Trough backarc basin: Geosphere, v. 17, https://doi.org/10.1130/GES02360.1.

Science Editor: Shanaka de Silva
Associate Editor: David W. Scholl

Received 8 October 2020
Revision received 22 March 2021
Accepted 20 May 2021



# Diffuse spreading, a newly recognized mode of crustal accretion in the southern Mariana Trough backarc basin

**Jonathan D. Sleeper[1], Fernando Martinez[2], Patricia Fryer[2], Robert J. Stern[3], Katherine A. Kelley[4], and Yasuhiko Ohara[5,6,7]**

[1]Mathematics, Natural, and Health Sciences Division, University of Hawai'i–West O'ahu, 91-1001 Farrington Highway, Kapolei, Hawai'i 96707, USA
[2]Hawai'i Institute of Geophysics and Planetology, School of Ocean and Earth Science and Technology, University of Hawai'i at Mānoa, 1680 East-West Road, POST 814A, Honolulu, Hawai'i 96822, USA
[3]Geosciences Department, University of Texas at Dallas, 800 W. Campbell Road, Richardson, Texas 75080, USA
[4]Graduate School of Oceanography, University of Rhode Island–Narragansett Bay Campus, Narragansett, Rhode Island 02882, USA
[5]Hydrographic and Oceanographic Department of Japan, Tokyo 100-8932, Japan
[6]Research Institute for Marine Geodynamics, Japan Agency for Marine-Earth Science and Technology, Yokosuka 237-0061, Japan
[7]Department of Earth and Planetary Sciences, Nagoya University, Nagoya 464-8601, Japan

## ABSTRACT

**South of the latitude of Guam, the Mariana Trough exhibits both trench-parallel and trench-normal extension. In this study, we examined the locus of trench-normal extension separating the Philippine Sea plate from the broadly deforming Mariana platelet. Along this boundary, we identified three distinct modes of extension and described their distinguishing characteristics using deep- and shallow-towed side-scan sonar and ship multibeam data along with regional geophysical, geochemical, and seismicity data. In the west, the Southwest Mariana Rift is an active tectonic rift exhibiting abundant strong earthquakes up to $m_b$ 6.7 and limited evidence of volcanism. In the east, the Malaguana-Gadao Ridge is a seafloor spreading center producing few and weak earthquakes less than $m_b$ 5. Between these zones, there is an ~20–40-km-wide and ~120-km-long area of high acoustic backscatter characterized by closely spaced volcano-tectonic ridges and small volcanic cones with distributed intermediate-strength seismicity up to $m_b$ 5.7. Fresh-looking volcanic rocks with high water contents and strong arc chemical affinities have been recovered from the high-backscatter zone. We interpret this morphologically and geophysically distinct zone as undergoing diffuse spreading, a distributed form of magmatic crustal accretion where new crust forms within a broad zone tens of kilometers across rather than along a narrow spreading axis. Diffuse spreading appears to be a rheological threshold effect enabled by slow opening rates and a high slab-fluid flux that facilitate the formation of a broad zone of weak hydrous lithosphere, within which new crust is accreted. Our findings describe a poorly understood process in plate tectonics, and observations of similar terrains in other backarc basins suggest that this process is not unique to the Mariana Trough.**

## INTRODUCTION

The Mariana Trough evolved though tectonic rifting of the predecessor volcanic arc beginning ca. 10 Ma, followed by magmatic accretion of new crust to form the backarc basin beginning ca. 5 Ma (Fig. 1; Karig, 1971, 1972; Karig et al., 1978; Hussong and Uyeda, 1981; Martinez et al., 1995; Fryer, 1996; Yamazaki et al., 2003; Stern et al., 2004). The rifting phase involved tectonic extension of preexisting arc crust, creating down-dropped tilted fault blocks that thinned the crust and deepened the seafloor. Rifting morphology is best exposed along the basin-facing edge of the remnant arc West Mariana Ridge (Figs. 1 and 2), whereas its eastern conjugate is now largely buried by Mariana Arc volcanism and volcaniclastic sediments (Karig, 1972; Scott and Kroenke, 1980, 1981; Oakley et al., 2009). The base of the eastern edge of the West Mariana Ridge often forms a local depth maximum (Fig. 2), followed by a typically abrupt transition (Figs. 2 and 3) to shallower seafloor with abyssal hill fabric and magnetic lineations that were formed by seafloor spreading (e.g., Yamazaki et al., 2003; Oakley et al., 2009; Seama and Okino, 2015). Early low-resolution single-beam bathymetric mapping made distinguishing the rifting to spreading transition ambiguous, and the transition was interpreted as extending significantly into the basin (e.g., Martinez et al., 1995). However, subsequent full-coverage high-resolution multibeam mapping, magnetic and gravity surveys, and seismic reflection profiles show clear abyssal hill fabric beginning near the base of the eastern slope of the West Mariana Ridge correlating with magnetic lineations and a rapid transition to higher mantle Bouguer anomalies in the basin (Yamazaki et al., 2003; Kitada et al., 2006; Oakley et al., 2009; Armstrong, 2011). These data indicate that, at least in the central Mariana Trough, basin opening was accommodated in two distinct predominant modes: (1) a narrow zone of tectonic rifting that transitioned rapidly to (2) focused magmatic seafloor spreading.

Mapping in other parts of the Mariana Trough has revealed more ambiguous terrains lacking either the block-faulted structure of tectonic rifts or the lineated abyssal hill fabric and magnetic anomalies formed by focused seafloor spreading. For example, in the northern Mariana Trough north of ~22°N, a zone of shallower seafloor lacking abyssal hill fabric is abruptly juxtaposed with clear seafloor spreading crust to the south (Baker et al., 1996). This contrast in morphology has led to the interpretation of the northern basin as a rifted terrain extending across the ~100 km width of the basin and to the northern apex of the trough (Stern et al., 1984; Yamazaki et al., 2003). More recent observations

Jonathan Sleeper https://orcid.org/0000-0002-0075-8474

in the southern Mariana Trough have shown broad expanses of the forearc that are actively extending magmatically but in a diffuse or distributed manner that does not resemble either seafloor spreading or tectonic rifting (Ribeiro et al., 2013; Martinez et al., 2018). These areas of unusual crustal fabric occur in regions that are expected to have a high slab-fluid flux (Schmidt and Poli, 1998), such as near-arc and forearc areas, and that are opening at slow rates (<45 mm/yr; Kato et al., 2003; "slow" designation based on Macdonald, 1982). The association of these diffuse terrains of crustal accretion with high slab-fluid flux and slow extension rates suggests that those parameters may be important controls on this process. Water, one of the primary components of slab fluids, has a strong weakening effect on olivine (Mei and Kohlstedt, 2000a, 2000b). Where mantle water contents are low, such as at mid-ocean ridges, melting beneath spreading centers effectively dehydrates the residual mantle. Dehydration by melting has been hypothesized to markedly strengthen the residual mantle, helping to focus the melt toward narrow plate-boundary zones (Hirth and Kohlstedt, 1996; Phipps Morgan, 1997). An opposing process may occur at subduction zones where water is continuously added through slab-derived fluids and strengthening due to dehydration is inhibited. In these regions, residual mantle in equilibrium with strongly hydrous melts retains appreciable water (Hirth and Kohlstedt, 2003), and the fluid flux from the slab may also rehydrate the residual material (Stolper and Newman, 1994; Martinez and Taylor, 2002). The plate-driven opening rate also affects the ability of mantle to dehydrate because it controls the flux of mantle through the melting regime and thus the rate of pressure-release mantle melting that extracts water. For a given flux of hydrous fluid from the slab, slower opening rates should yield more hydrous mantle as the available water is distributed within a smaller total volume of mantle. Thus, backarc settings opening above dewatering slabs have variably hydrous residual mantle depending on both the fluid flux from the slab and the rate of plate-driven mantle advection though the melting regime. These processes could profoundly affect the mantle's ability to form the narrow plate-boundary zones that characterize seafloor spreading.

To investigate the possible existence of a diffuse mode of magmatic crustal accretion in backarc basins underlain by a dewatering slab, we examined the divergent boundary in the Mariana Trough south of about the latitude of Guam (Fig. 2). In this part of the basin, the trench curves to the west and becomes increasingly oriented in the direction of trough opening (Fryer et al., 1998; Kato et al., 2003), creating a strong component of trench-parallel extension within the Mariana platelet forearc (Martinez et al., 2000, 2018) that is separate from the trench-normal extension in the backarc basin. The divergent boundary in the backarc curves westward in concert with the trench, and its morphology changes from the magmatically robust seafloor spreading center of the Malaguana-Gadao Ridge (Martinez et al., 2000; Becker et al., 2010) in the northeastern part of our study area to a predominantly tectonic rift at the narrow (~40 km) Southwest Mariana Rift (Becker, 2005; Wan et al., 2019) in the west (Figs. 2 and 3). These extensional domains are separated by a distinct ~120-km-long and ~20–40-km-wide volcano-tectonic terrain of crustal accretion that we call the diffuse spreading zone (Figs. 2 and 3; Martinez et al., 2018).

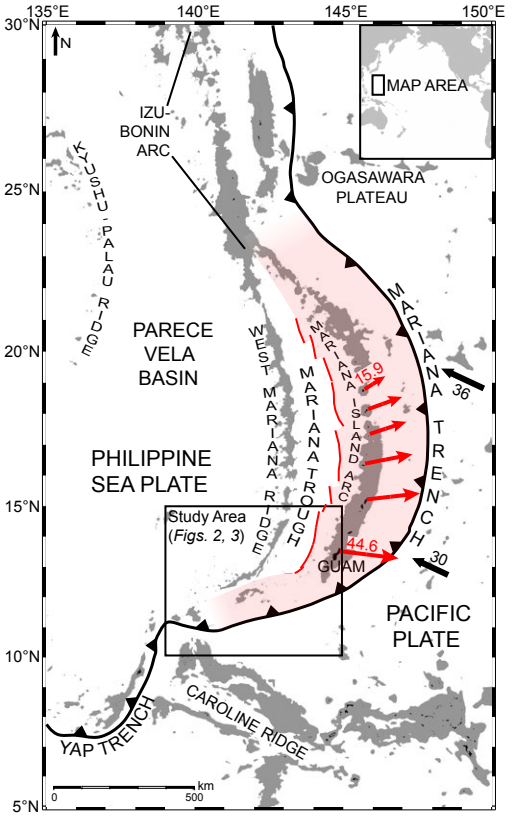


**Figure 1. Simplified regional map using ETOPO1 arc-minute global relief data (Amante and Eakins, 2009). Gray areas indicate seafloor shallower than 2500 m; black indicates islands. Major tectonic and volcanic features are labeled, identified spreading axes in the Mariana Trough are marked with red lines, and the trench is marked with a bold black line, with triangles on the upper plate. Mariana platelet is shown with light red shading; the northern and southern borders are diffuse and/or uncertain. Global positioning system (GPS) vectors from Kato et al. (2003) are marked with red arrows (Mariana arc relative to Philippine Sea plate) and black arrows (Pacific plate relative to the Philippine Sea plate), and all velocities are in mm/yr.**

In this study, we described the geophysical, seismotectonic, and geochemical characteristics of the diffuse spreading zone, focusing on the contrasts with rifting and focused spreading, typified by the Southwest Mariana Rift and Malaguana-Gadao Ridge, respectively. The descriptions were based on multibeam and deep-towed sonar data collected in December 2011 to January 2012 aboard R/V *Thomas G. Thompson* combined with publicly available multibeam

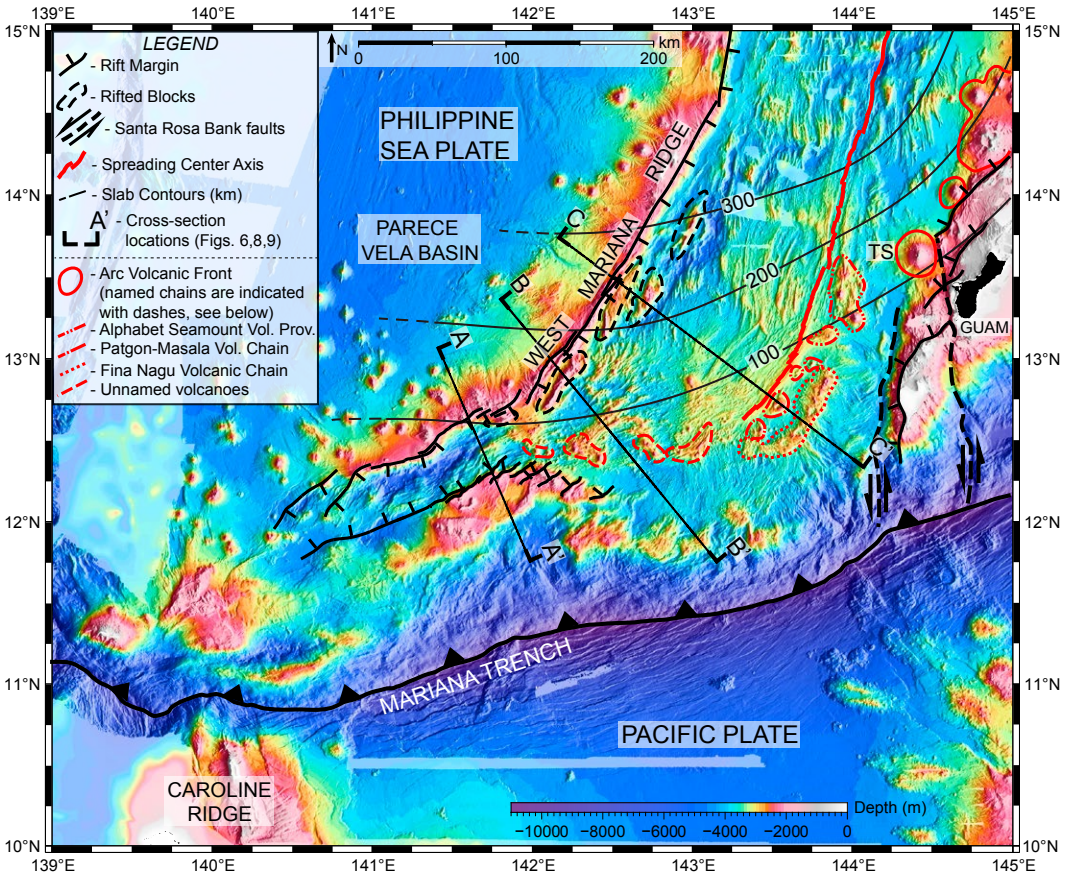


**Figure 2. Compiled bathymetric map (0.001° cell size, ~100 m) of the southern Mariana region showing the relevant tectonic and volcanic features; see legend for symbols. The portion of the arc volcanic front marked with various dashed red lines is characterized by disrupted, immature, or possibly extinct arc volcanoes; see section in text on "Volcanism in the Southern Mariana Region" for description. Gaps in multibeam coverage in this and subsequent bathymetric maps were filled with predicted bathymetry from satellite altimeter measurements (lighter shading; Smith and Sandwell, 1997). TS—Tracey Seamount. Slab contours are from the Slab 2.0 model (Hayes et al., 2018). Cross-section A-A′ is shown in Figure 6C, B-B′ is shown in Figure 8C, and C-C′ is shown in Figure 9C.**

and shallow-towed sonar, gravity, and seismicity data. These descriptions and associated analyses were used to support our hypothesis that the diffuse spreading zone was formed by a distinct distributed mode of magmatic crustal accretion enabled by high slab-fluid flux and slow opening rates. Similar terrains in other backarc basins suggest that diffuse spreading likely occurs elsewhere, but it is not widely recognized as a distinct mode of crustal accretion.

## GEOLOGIC BACKGROUND: SOUTHERN MARIANA REGION

### Southern Mariana Trough Opening and Tectonics

In the southern Mariana Trough (Figs. 2 and 3), the Southwest Mariana Rift, diffuse spreading zone, and Malaguana-Gadao Ridge form a continuous divergent boundary between the Philippine Sea plate to the north and west and the deforming Mariana platelet to the south and east (Fig. 1; Martinez et al., 2000, 2018). Though there is evidence of relatively recent deformation and possibly volcanism along the eastern base of the West Mariana Ridge near 17°50′N (Fryer, 1995), we consider the western Mariana Trough, the West Mariana Ridge, and the Parece Vela Basin to be a part of a single rigid Philippine Sea plate that extends to the convergent boundaries along East Asia, as defined geodetically (Seno et al., 1993; Kato et al., 2003) and based on the known plate boundaries (Bird, 2003). Thus, we interpret the fabric of magmatic crust accreted onto the NW flank of the diffuse spreading zone and Malaguana-Gadao Ridge (i.e., Philippine Sea plate side) to record the configuration of the extensional zones at the time of formation (Martinez et al., 2000, 2018; Seama and Okino, 2015). In contrast, in the forearc to the south and east, the Mariana platelet (shaded in red in Fig. 1) is actively deforming, as indicated by distributed earthquakes

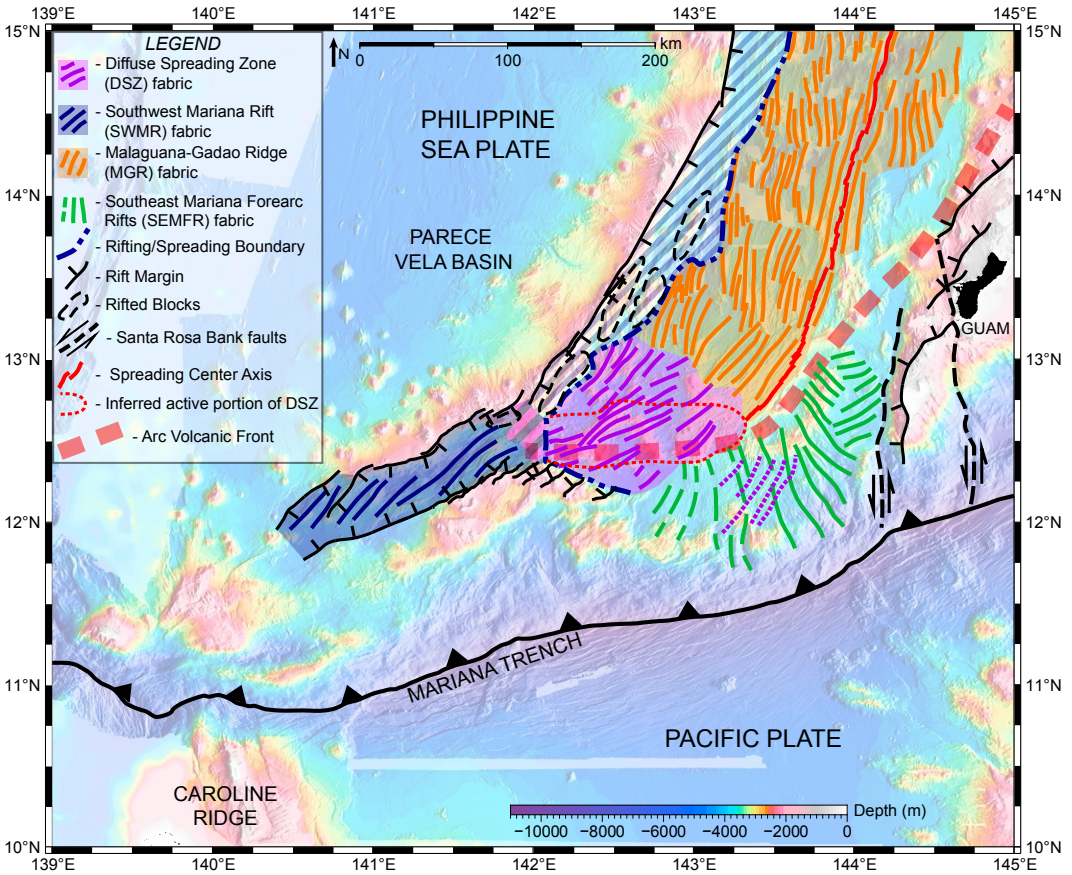


**Figure 3. Generalized map of southern Mariana Trough seafloor fabric with major volcanic and tectonic lineations mapped. Four regimes were recognized from seafloor morphology and are color-coded: 1—Southwest Mariana Rift (blue), where blue striped zone indicates inactive rift fabric along the eastern flank of the West Mariana Ridge. Purple and blue stripes indicate a short transition zone between the Southwest Mariana Rift and the diffuse spreading zone to the east. 2—Diffuse spreading zone (purple), where dotted purple lines indicate aligned fabric within the forearc outside of the diffuse spreading zone. Portion outlined with red dashed line is the inferred active part of the diffuse spreading zone that corresponds to the high acoustic backscatter (Fig. 5B) and recent seismicity (Fig. 7B). 3—Focused spreading along the Malaguana-Gadao Ridge (orange). 4—Southeast Mariana forearc rift (SEMFR, green, not the focus of this study). Dashed green lines to the west indicate the largely inactive portion of the forearc that underwent similar extension in the past (Martinez et al., 2018). The arc volcanic front is depicted schematically here with a thick dashed red line to show that the arc and locus of extension generally converge toward the southwest. The boundary between rifted and spread crust, interpreted based on the morphology, is shown with a dashed blue line. See legend for other symbols.**

and finely spaced tectono-magmatic seafloor fabric oriented at high angles to the trend of the Malaguana-Gadao Ridge/diffuse spreading zone and the trench (generalized fabric shown in green and labeled on Fig. 3; Martinez et al., 2000, 2018; Fryer et al., 2003; Ribeiro et al., 2013). This high-angle fabric reaches close to the Malaguana-Gadao Ridge/diffuse spreading zone divergent boundary, indicating it is continually formed soon after spreading away from the boundary. Earthquake tension axes here are subparallel to the trench and approximately orthogonal to those in the Southwest Mariana Rift and diffuse spreading zone, indicating a separate component of trench-parallel extension in the forearc (Martinez et al., 2018).

Farther west, the flanks of the Southwest Mariana Rift are composed of the remnant arc West Mariana Ridge to the north, which has been rifted away from the Eocene–Miocene forearc terrain that forms the Mariana platelet to the south (Figs. 1, 2, and 3). In this area, the forearc has not undergone extensive trench-parallel extension and forms a fairly cohesive unit from the termination of the Mariana Trench near 139°E to ~142°E. Within the Southwest Mariana Rift, tectonic deformation, evidenced by numerous extensional earthquakes, is focused within an ~40-km-wide valley formed by down-dropped fault blocks. The narrowing of the basin from over 100 km in the diffuse spreading zone to 40 km in the Southwest Mariana Rift suggests that opening rates are decreasing westward. The Southwest Mariana Rift fabric (labeled on Fig. 3), defined by the major faults, is rotated ~15°–20° counterclockwise relative to an implied trench-normal extension direction and the overall trend of the rifted margins. This observed fault obliquity is consistent with numerical modeling (Brune et al., 2012) predicting that, in the early stages of tectonic rifting, it is mechanically preferred for extensional strain to accumulate on oblique structures.

East of the Southwest Mariana Rift, between ~142°E and 144°15′E, the preexisting Eocene–Miocene forearc has been rifted apart with only a few

high-standing remnant blocks remaining (Fig. 2; Reagan et al., 2018; Stern et al., 2020). Most of the forearc here consists of newly magmatically accreted material <4 m.y. old (Ribeiro et al., 2013, 2015; Stern et al., 2014, 2020; Martinez et al., 2018). The conjugate margin of the Eocene–Miocene rifted forearc in the east is marked by two active left-lateral transtensional faults, the West Santa Rosa Bank fault and the East Santa Rosa Bank fault, SSW of Guam near 144°15′E and 144°40′E, respectively (Fig. 2; Fryer et al., 2003).

## Volcanism in the Southern Mariana Region

The southern Mariana region differs significantly from the region to the north. The central Mariana Trough between ~14°N and 19°N lies west of a mature arc volcanic front (Bloomer et al., 1989; Baker et al., 2008) and the ~200-km-wide forearc (Stern and Smoot, 1998) (Fig. 1), which hosts numerous serpentinite mud volcanoes (Fryer et al., 1985, 1998; Fryer, 2012). Focused crustal accretion occurs along the Mariana Trough spreading center, which is defined by a narrow axial valley with both transform and nontransform offsets between segments, morphologically similar to slow-spreading mid-ocean ridges (Kong, 1993; Seama and Fujiwara, 1993). Beneath the central Mariana Trough north of 14°22′N, the slab dips steeply and does not underlie the spreading axis, whereas in the south, the slab dips more gently and underlies the axis and much of the backarc basin (Fig. 2; Hayes et al., 2018; Zhu et al., 2019).

As the slab depths beneath the spreading center decrease and the locus of extension approaches the arc southward (Fig. 3), the morphology of the spreading center changes significantly. South of about the latitude of Guam (13°30′N), the spreading center is the Malaguana-Gadao Ridge, forming a magmatically robust axial high (solid red line in Fig. 2) similar to a fast-spreading mid-ocean ridge (Martinez et al., 2000; Becker et al., 2010), despite slow spreading rates (Macdonald, 1982) of ~40–45 mm/yr (Kato et al., 2003; Seama and Okino, 2015). The transition from axial valley to axial high is similar to other backarc basins with spreading axes near the arc volcanic front, e.g., the Scotia backarc basin (Livermore et al., 1997), the Lau Basin (Martinez and Taylor, 2002; Martinez and Taylor, 2006; Dunn and Martinez, 2011; Sleeper and Martinez, 2014; Sleeper et al., 2016), and the Manus Basin (Taylor and Martinez, 2003). Consistent with the magmatically robust character of the Malaguana-Gadao Ridge, the trough crust south of ~14°22′N is thicker (5.9–6.9 km on average) compared to that farther north (3.4–4.1 km on average), based on gravity modeling (Kitada et al., 2006). The thicker crust persists south of ~14°22′N, from the West Mariana Ridge to the Malaguana-Gadao Ridge, and extends west to the Southwest Mariana Rift (Kitada et al., 2006), although somewhat thinner crust (by up to 1.9 km) may characterize the southern Mariana forearc, based on depth and gravity analyses (Martinez et al., 2018). An ocean-bottom seismic refraction survey across the Malaguana-Gadao Ridge (Sato et al., 2015) showed similar crustal structure to the Valu Fa Ridge in the Lau Basin (Dunn and Martinez, 2011), with upper-crustal seismic velocities that are lower than typical for mid-ocean ridges. The distinctive seismic structure of the thick arc-proximal crust in the Lau Basin has been inferred to be related to increased mantle hydration from the slab, leading to greater melting and a more porous and differentiated upper crust than at mid-ocean ridges (Dunn and Martinez, 2011; Dunn et al., 2013; Arai and Dunn, 2014; Eason and Dunn, 2015). These observations document the abrupt effects of arc proximity on mantle hydration and consequent crustal production, structure, morphology, and chemistry (Martinez and Taylor, 2003; Taylor and Martinez, 2003; Dunn and Martinez, 2011; Sleeper and Martinez, 2014; Sleeper et al., 2016).

Along with the contrasts observed in the backarc spreading center, there are also abrupt changes in the arc volcanic front in the southern Mariana Trough. Southwest of Guam, where the Eocene–Miocene forearc is undergoing approximately E-W extension between 142°E and 144°15′E (Fig. 2; Martinez et al., 2000, 2018; Kato et al., 2003; Ribeiro et al., 2013), there is a corresponding change in the morphology of the arc volcanic front (Fryer et al., 1998; Stern et al., 2013; Masuda and Fryer, 2015; Brounce et al., 2016). At Tracey Seamount, ~30 km northwest of Guam (labeled "TS" on Fig. 2), and along the arc toward the north, the arc volcanoes form conical edifices ~30–100+ km in diameter (solid red outlines in Fig. 2), reaching depths shallower than 1000 m in many cases, and forming volcanic islands farther north along the chain (Bloomer et al., 1989; Baker et al., 2008). In contrast, the arc volcanoes flanking the Malaguana-Gadao Ridge axis to the west and south are much smaller (indicated by dashed outlines on Fig. 2, where different dash styles correspond to different volcanic chains/clusters [see legend]), with diameters of <10 km and minimum summit depths of ~1800 m. Some of the volcanoes have been affected by extensional faulting (Fryer et al., 1998), and possibly withdrawal of melt by the adjacent Malaguana-Gadao Ridge (Becker et al., 2010). The Alphabet Seamount volcanic province (Fryer et al., 1998; Stern et al., 2013) and volcanoes adjacent to the Malaguana-Gadao Ridge, the Patgon-Masala volcanic chain (Masuda and Fryer, 2015), are relatively less faulted than the Fina Nagu volcanic complex (Brounce et al., 2016) farther from the Malaguana-Gadao Ridge. Arc volcanic front edifices (Pearce et al., 2005) become less distinct southwest of the Malaguana-Gadao Ridge axis, forming clusters of larger volcanic cones along the southern margin of the diffuse spreading zone ("Unnamed" volcanoes in Fig. 2). With no focused spreading axis in the diffuse spreading zone and evidence of extension in the elongate morphology of some of the arc volcanoes, it appears that the loci of backarc extension and arc volcanism are at least partly overlapping in the diffuse spreading zone (Fig. 3).

Based on the seismically determined position of the slab (contours from the Slab 2.0 model; Hayes et al., 2018; Fig. 2), the Malaguana-Gadao Ridge south of 13°05′N, the diffuse spreading zone, and the Southwest Mariana Rift overlie the Pacific slab at depths of 100 km or less. A local ocean-bottom seismometer study centered over the Southwest Mariana Rift and the forearc found somewhat deeper slab depths in some areas >~80 km from the trench, but also confirmed the presence of the slab beneath the Malaguana-Gadao Ridge and diffuse spreading zone (Zhu et al., 2019). In this setting, abundant slab dewatering is predicted by studies of the metamorphic breakdown of hydrous

minerals (Peacock, 1990; Schmidt and Poli, 1998), leading to enhanced melt production. Consistent with their position close to the arc volcanic front, high water content of lava samples has been reported in several locations along the Malaguana-Gadao Ridge and from a small cone within the diffuse spreading zone (Brounce et al., 2014; Masuda and Fryer, 2015; Martinez et al., 2018). Figure 4 shows the locations of these and other relevant samples collected and analyzed by others. Masuda and Fryer (2015) reported measured water contents of samples from the Malaguana-Gadao Ridge of ~2 wt% (1.9%–2.1%) between 13°05′N and 13°06′N, and 1.2%–1.5% to the north at 13°12′N. Of the samples reported in Brounce et al. (2014) from the Malaguana-Gadao Ridge and diffuse spreading zone, the measured water contents of the diffuse spreading zone samples (1.5% and 1.9%) fall within the range of the Malaguana-Gadao Ridge samples (1.5%–2.5%), but one of the diffuse spreading zone samples showed higher calculated mantle water content (0.3%) and higher melt fraction (21%) compared to the Malaguana-Gadao Ridge samples (0.19%–0.25% and 12%–15%, respectively; Fig. 4). Although the number of samples is limited, higher mantle water contents in the diffuse spreading zone are consistent with a position above the dewatering slab and decreasing opening rates relative to the Malaguana-Gadao Ridge.

Additional volcanic rock samples were dredged throughout the diffuse spreading zone region in 2006 (Masuda, 2006) (green stars in Fig. 4). The samples were all described as basaltic lavas, many with quenched glass, and particularly fresh lavas from the eastern portion of the region ~15 km west of the Malaguana-Gadao Ridge terminus, though no published analyses are available. Dredged samples from one of the volcanic cones south of the shallow platform at ~142°E (westernmost red triangle in Fig. 4) recovered fresh, glassy lavas with arc-like compositions (Becker, 2005; Pearce et al., 2005), indicating recent volcanic activity there. The lack of cones to the west within the Southwest Mariana Rift suggests that this is the western terminus of active arc-type volcanism within the Mariana Trough.

In the Southwest Mariana Rift itself, the Japan Agency for Marine-Earth Science and Technology (JAMSTEC) conducted *Shinkai 6500* (manned submersible) dives 1400 and 1401 during the YK14–13 cruise in 2014 (Ohara et al., 2014). These dives recovered basalts and gabbro with both backarc and arc affinities based on trace-element analyses from the eastern part of the rift near 141°41′E and 141°34′E, respectively (magenta rectangles in Fig. 4). Refraction velocities from an active-source ocean-bottom seismometer experiment crossing the Southwest Mariana Rift (Wan et al., 2019) have been interpreted as indicating serpentinized upper-mantle material beneath the rift, which implies that temperatures are too low to sustain active magmatism, although slab dewatering likely occurs beneath this area as well.

## METHODOLOGY: GEOPHYSICAL DATA SETS AND PROCESSING

Bathymetric maps were created using a regional multibeam data set from the University of New Hampshire Center for Coastal and Ocean Mapping/Joint Hydrographic Center (UNH/CCOM-JHC) Law of the Sea expeditions (Armstrong, 2011), supplemented with data from the National Centers for Environmental Information (NCEI, ngdc.noaa.gov), the Japan Agency for Marine-Earth Science and Technology (JAMSTEC, godac.jamstec.go.jp), and R/V *Thomas G. Thompson* cruise TN273 (22 December 2011–22 January 2012). The final multibeam compilation included data collected during 43 expeditions from the NCEI database and 11 expeditions from the JAMSTEC database, omitting only data

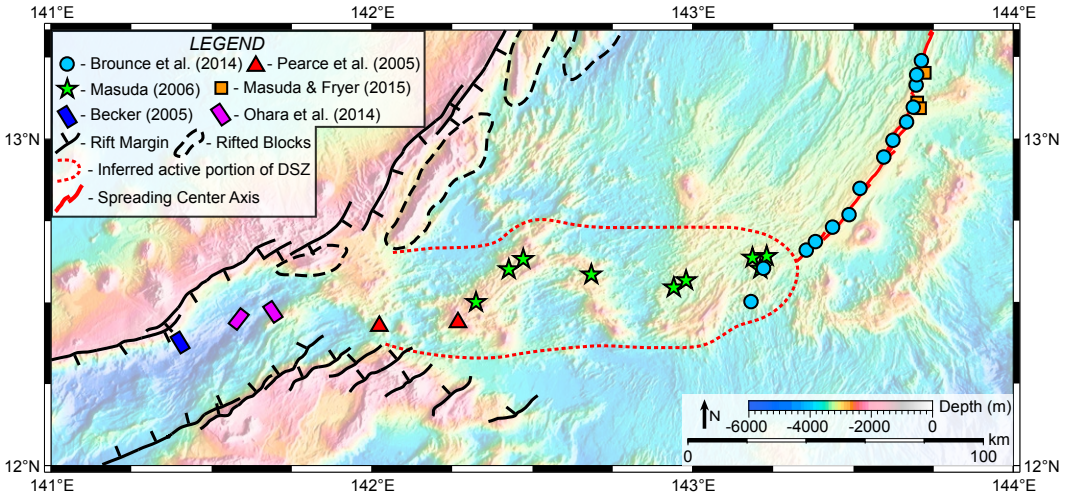


**Figure 4. Locations of relevant rock samples collected and analyzed by others. Background bathymetry map was made from the compiled regional grid (0.001° cell size, ~100 m) used for Figures 2 and 3. References and symbols are shown in the legend. DSZ—diffuse spreading zone.**

that added noise without increasing the coverage area. During the TN273 expedition, a deep-towed side-scan sonar survey using a 30 kHz IMI-30 instrument (Rognstad, 2005) covered the southernmost portion of the Malaguana-Gadao Ridge axis and a small area southwest of the axis, providing high-resolution imagery (gridded at 0.00003° or ~3 m) of fine-scale volcanic and tectonic structures. Due to the limited coverage area of the deep-towed survey, the regional side-scan sonar map was created from a combined grid of two HMR-1 (Rognstad, 1992) shallow-towed side-scan sonar surveys in 1997 on R/V *Moana Wave* (MW9719) and in 2001 on R/V *Melville* (COOK06MV) (Martinez et al., 2000; Fryer et al., 2003). Compiled multibeam backscatter data from the UNH/CCOM-JHC Law of the Sea expeditions (Armstrong, 2011) were used to fill in around the HMR-1 survey areas.

Gravity data from shipboard gravimeters were also compiled from both the NCEI and JAMSTEC databases, and these were used to calculate the mantle Bouguer anomaly (Kuo and Forsyth, 1988) using GMT software (Wessel et al., 2019). Gaps in both the multibeam and gravity data sets were filled with predicted bathymetry (Smith and Sandwell, 1997) and gravity (Sandwell et al., 2014) from satellite altimeter measurements. The mantle Bouguer anomaly was calculated by removing the gravitational effects of nominal 6-km-thick crust (Kuo and Forsyth, 1988) from the Bouguer anomaly, using densities of 1035 kg/m$^3$ for water, 2700 kg/m$^3$ for crust, and 3300 kg/m$^3$ for mantle. The crustal density and thickness values were chosen to approximate the density and thickness of the young backarc crust in the southern Mariana Trough. The gridded gravity data and bathymetry data were resampled in a 2048 × 2048 cell grid, with a resultant cell spacing of ~270 m (0.00244°), and five terms were used in the Fourier series of the Parker method (Parker, 1972). The resulting mantle Bouguer anomaly contained an expected signal from the underlying slab, but the slab is 60 to >100 km deep in most of this area, so the gravity effect has low amplitude and long wavelength (Watts and Talwani, 1975). This long-wavelength signal does not significantly affect our qualitative interpretations of the shorter-wavelength and higher-amplitude crustal signal in the backarc region.

Earthquake focal mechanisms were obtained from the Harvard Centroid Moment Tensor (CMT) catalog (Dziewonski et al., 1981; Ekström et al., 2012), along with locations of earthquakes (limited to body-wave magnitude 4 or greater) from the International Seismological Centre (ISC) reviewed event catalogue (International Seismological Centre, 2020). Depth was limited to 51 km to isolate upper-plate earthquakes. The data set was also limited to 1962 or later, when the seismic network was sufficient to precisely locate the events, with the exception of one large ($m_b$ 6.7), well-located event in 1935 on the northern flank of the Southwest Mariana Rift. The total seismic moment discussed in the section on "Seismicity in the Southern Mariana Trough" was calculated by first converting body-wave magnitude ($m_b$) to moment magnitude ($M_w$) using the formula derived from global earthquake observations by Scordilis (2006):

$$M_w = 0.85(\pm 0.04)m_b + 1.03(\pm 0.23). \quad (1)$$

The moment magnitude for each event was then converted to seismic moment ($M_0$) in dyn-cm using a formula derived from Kanamori (1977):

$$M_0 = 10^{(1.5 \times M_w + 16.1)}. \quad (2)$$

The total moment was then simply obtained as the sum of the moments for each of the groups of earthquakes considered.

## OBSERVATIONS AND RESULTS

The multiple mapping instruments used and their nested resolutions provided a good assessment of the variations in volcano-tectonic morphologies along the southern Mariana divergent boundary. The evidence for distinct extensional processes and abrupt transitions between the diffuse spreading zone, Malaguana-Gadao Ridge, and Southwest Mariana Rift came primarily from contrasts in seafloor morphology and seismicity. Below, we describe the characteristic seafloor morphology and seismicity associated with rifting in the Southwest Mariana Rift, focused spreading along the Malaguana-Gadao Ridge, and what we interpret as diffuse spreading in the intervening diffuse spreading zone, focusing on the contrasts and features that indicate distinct modes of extension in each of the three regions. Multibeam bathymetry maps and backscatter imagery of the entire study area are presented in Figure 5, while detailed maps and cross sections for each of the three focus areas are introduced in the following sections.

### Southwest Mariana Rift Morphology

The Southwest Mariana Rift (Fig. 6) is characterized by an ~40-km-wide graben up to 5500 m deep in places, bounded by steep faulted margins with up to 3500 m of relief from the rift floor to the top of the uplifted rift margins. Similar rift-type morphology, consisting of down-dropped blocks separated by steep inward-facing escarpments (the largest of which are outlined on Figs. 2–5 and 7A), is present outside of the active Southwest Mariana Rift in an ~20–40-km-wide zone along the eastern flank of the West Mariana Ridge (blue striped zone in Fig. 3), but these features do not extend basinward to the diffuse spreading zone or Malaguana-Gadao Ridge flanks. The narrow zone of fault-block morphology along the eastern West Mariana Ridge implies a distinct rifting phase that rapidly transitions into a different mode of extension in the diffuse spreading zone, or to focused seafloor spreading along the Malaguana-Gadao Ridge flanks. A characteristic of the transition from rifting to spreading is an abrupt morphologic change from deepened and thinned preexisting arc crust to a more uniform seafloor depth and crustal thickness in the younger seafloor formed through magmatic crustal accretion (e.g., Fryer and Hussong, 1981; Taylor et al., 1999; Oakley et al., 2009).

The Southwest Mariana Rift is asymmetric (Figs. 6A and 6C) in profile. The northwest margin is typically characterized by a single normal fault scarp with

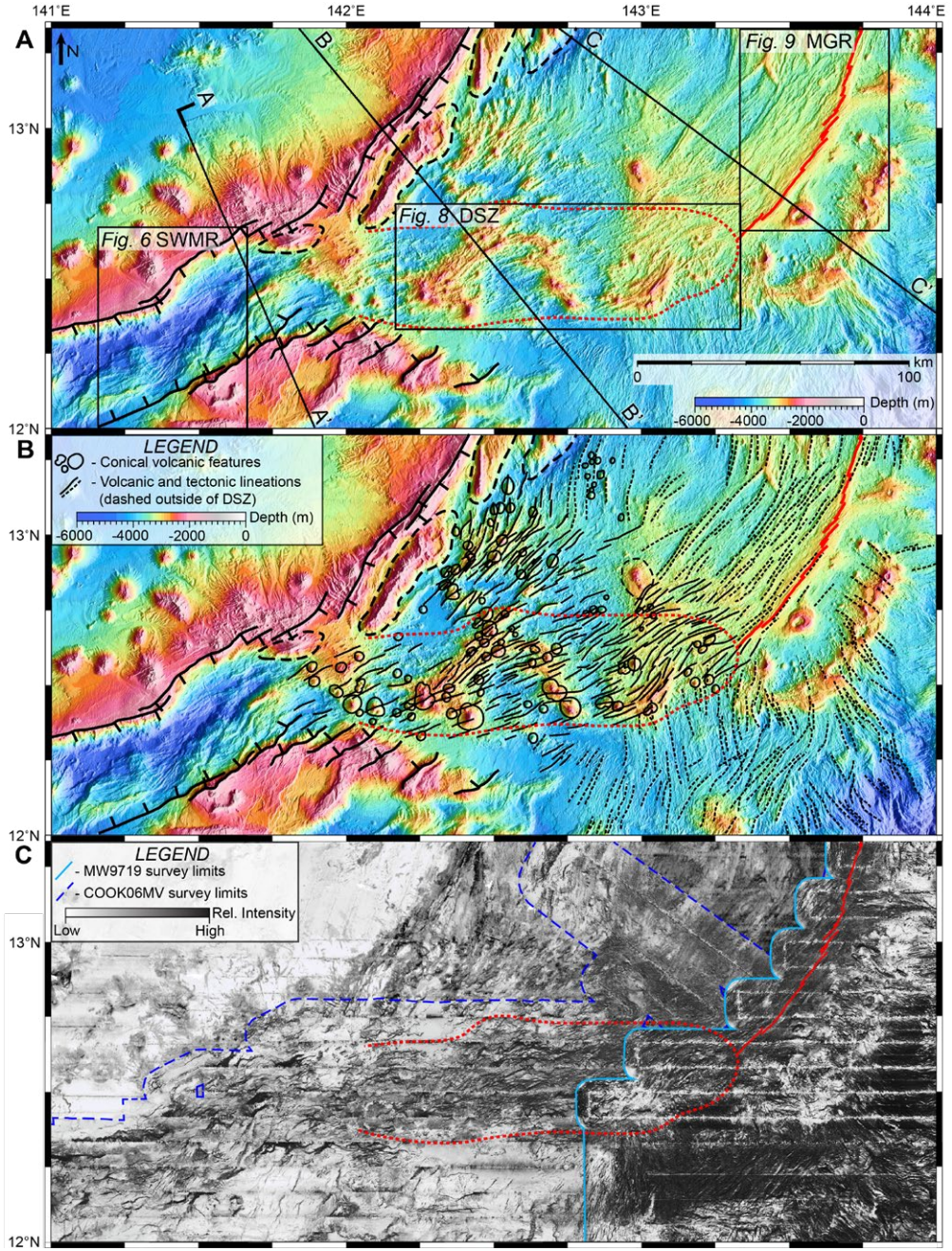


**Figure 5. Multibeam bathymetry maps and acoustic backscatter imagery of the entire study area. (A) Compiled bathymetry map (0.001° cell size, ~100 m) showing location of focus areas and cross sections in Figures 6, 8, and 9. DSZ—diffuse spreading zone; MGR—Malaguana-Gadao Ridge; SWMR—Southwest Mariana Rift. (B) Interpreted bathymetric map showing detailed mapping of tectonic and volcanic lineations and conical volcanic features. See legend for symbols. (C) Compiled sonar backscatter map (0.001° cell size, ~100 m) showing both HMR-1 shallow-towed surveys (solid light blue line—MW9719 survey limits, dashed blue line—COOK06MV survey limits), with the background filled in using the University of New Hampshire Center for Coastal and Ocean Mapping/Joint Hydrographic Center (UNH/CCOM-JHC) Law of the Sea compiled multibeam backscatter data (Armstrong, 2011). Distance scale in A applies to all three panels.**

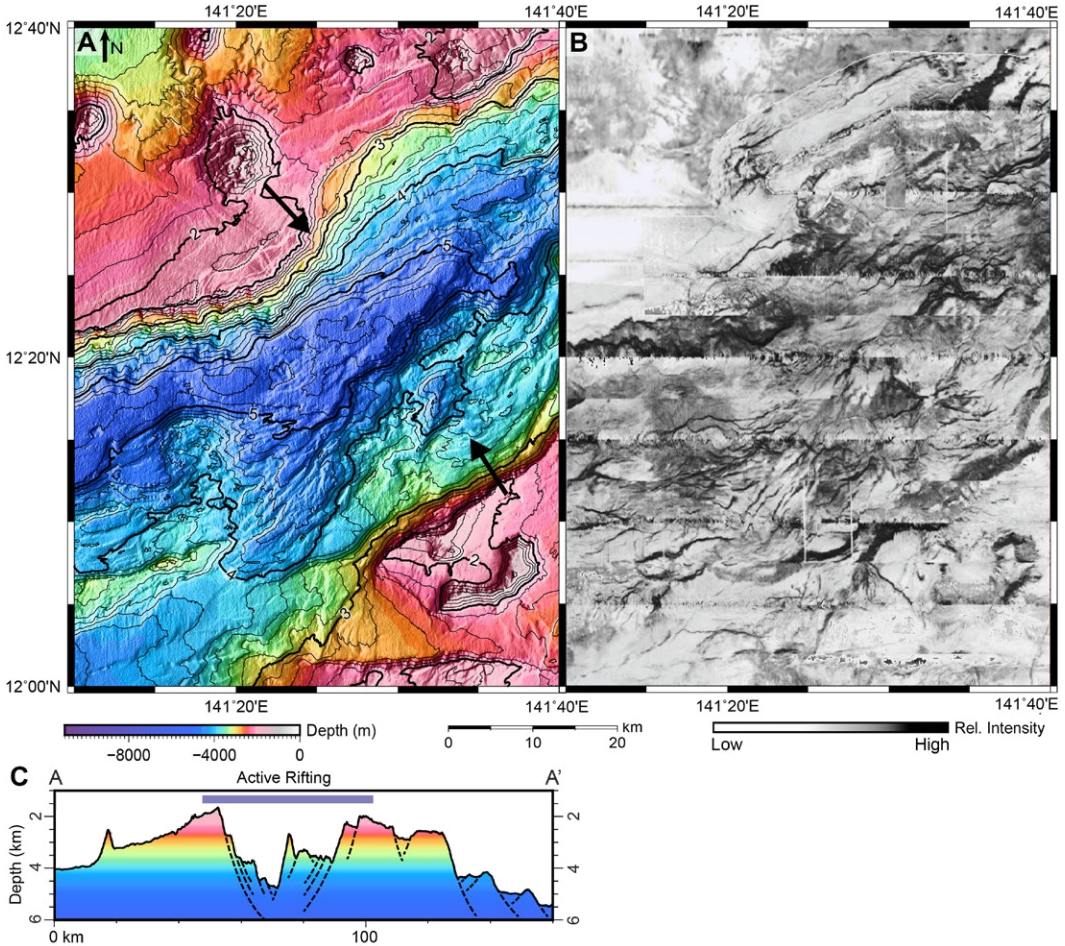


**Figure 6. Southwest Mariana Rift (SWMR) focus area; see Figure 5 for regional context. (A) Compiled bathymetry map (0.0003° cell size, ~30 m) showing Southwest Mariana Rift morphology. Contour interval = 0.2 km (200 m); contour lines are bold and labeled every 1 km. Locations indicated by the black arrows are discussed in section of text on "Southwest Mariana Rift Morphology." (B) Compiled acoustic backscatter imagery (0.001° cell size, ~100 m). (C) A-A′: Cross section (~7× vertical exaggeration) through the active rift valley, with some of the major rift faults schematically mapped based on the surface topography. Cross-section location is shown on Figures 2 and 5A. See section on "Southwest Mariana Rift Morphology" for detailed description.**

relief of >3000 m that in places splays into multiple surface traces. An example is indicated in Figure 6A with a black arrow along the northwest margin where it transitions from a single trace to the west to multiple traces to the east. The southeast margin is more irregular and faulted, and there is a large heavily deformed block (marked with a black arrow in Fig. 6A along the southeast margin) between the outermost fault scarp and the deepest part of the rift, causing the southeast margin to step down in several blocks rather than as a single steep scarp intersecting the valley floor (Fig. 6A). The backscatter image in Figure 6B (shown in regional context in Fig. 5C) shows generally low backscatter intensities within the Southwest Mariana Rift consistent with sediment-covered fault blocks and a general lack of recent volcanism, interspersed with irregular lineations interpreted as fault scarps, which appear as either shadows or strong reflections depending on the ensonification direction of the sonar. Although there is no clear evidence of recent volcanism within the rift graben based on the generally low backscatter, the lack of volcanic cones or lava-flow morphologies, and the sparse samples that have been recovered, we cannot rule out minor fault-controlled volcanism in localized areas. As noted earlier, seismic refraction data indicate somewhat low velocities beneath the Southwest Mariana Rift, but these have been interpreted as serpentinized material rather than high temperatures or melt (Wan et al., 2019).

The mantle Bouguer anomaly of the Southwest Mariana Rift (Fig. 7A) is consistent with crustal thinning of the remnant arc and forearc margins, with broad lows associated with the thick arc/forearc crust (~–90 to –130 mGal) abruptly transitioning to higher values (~–45 to –90 mGal) within the rift valley. At the eastern end of the Southwest Mariana Rift near ~142°E, small volcanic cones overlying a local topographic high resemble those found in the diffuse spreading zone to the east. However, this area has lower gravity anomalies than the diffuse spreading zone (~–65 to –90 mGal; Fig. 7A), indicating that the volcanic cones may be superimposed on thicker preexisting crust. Two earthquakes with normal fault mechanisms (Fig. 7B) indicate ongoing tectonic rifting here as well. Given the mixture of both Southwest Mariana Rift and diffuse spreading zone characteristics in this location, it appears to be a short transition zone between the Southwest Mariana Rift and diffuse spreading zone (magenta and blue striped zone in Fig. 3).

## Diffuse Spreading Zone Morphology

Within the diffuse spreading zone, the fault-block controlled morphology of the Southwest Mariana Rift is replaced by a terrain characterized by kilometer-scale volcanic ridges and cones, with much smaller, closely spaced faults (Fig. 8A). Diffuse spreading zone terrain extends from 142°05′E to the

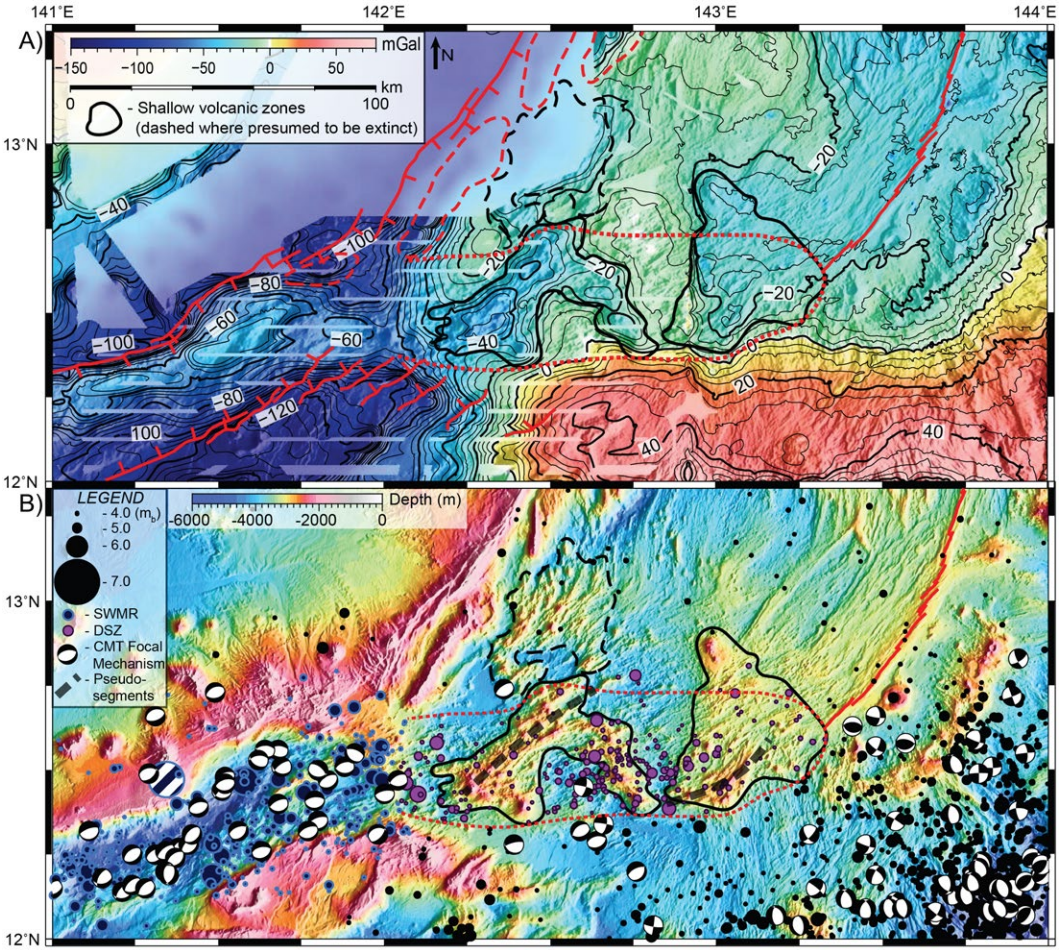


**Figure 7. (A) Mantle Bouguer anomaly (MBA) map of the study area, calculated by removing the effects of the bathymetry and of 6-km-thick young oceanic crust from the free-air anomaly; see "Methodology" section for details on processing. Warm colors indicate positive anomalies, and cool colors indicate negative anomalies. Black outlines delineate localized areas of elevated volcanic topography (dashed line indicates presumed inactive features within the low-backscatter zone in Fig. 5B), showing that the shallow volcanic features occur in discrete zones rather than being evenly distributed throughout the diffuse spreading zone. Contour interval = 5 mGal. Note that there are small localized spikes that were not removed in the compiled data set at 142°55′E, 12°23′–27′N (anomalous positive [yellow] values). (B) Compiled bathymetry map (0.001° cell size, ~100 m) overlaid with seismicity data from both the International Seismological Centre (International Seismological Centre, 2020) and Harvard Centroid Moment Tensor (CMT) catalogs (Dziewonski et al., 1981; Ekström et al., 2012). Blue circles indicate earthquakes within the Southwest Mariana Rift, purple circles indicate earthquakes within the active portion of the diffuse spreading zone (outlined with red dashed line), and black circles indicate earthquakes outside of the diffuse spreading zone and Southwest Mariana Rift. Thin black lines surround the zones of shallow volcanic topography, also shown in Figure 7A. Thick black dashed lines mark the locations of pseudo-segments that are described in "Malaguana-Gadao Ridge Spreading Morphology" section and discussed in "Possible Diffuse Spreading Mechanisms" section of the text. See legend for symbols and section of the text on "Seismicity in the Southern Mariana Trough" for analysis of seismicity. DSZ—diffuse spreading zone; SWMR—Southwest Mariana Rift.**

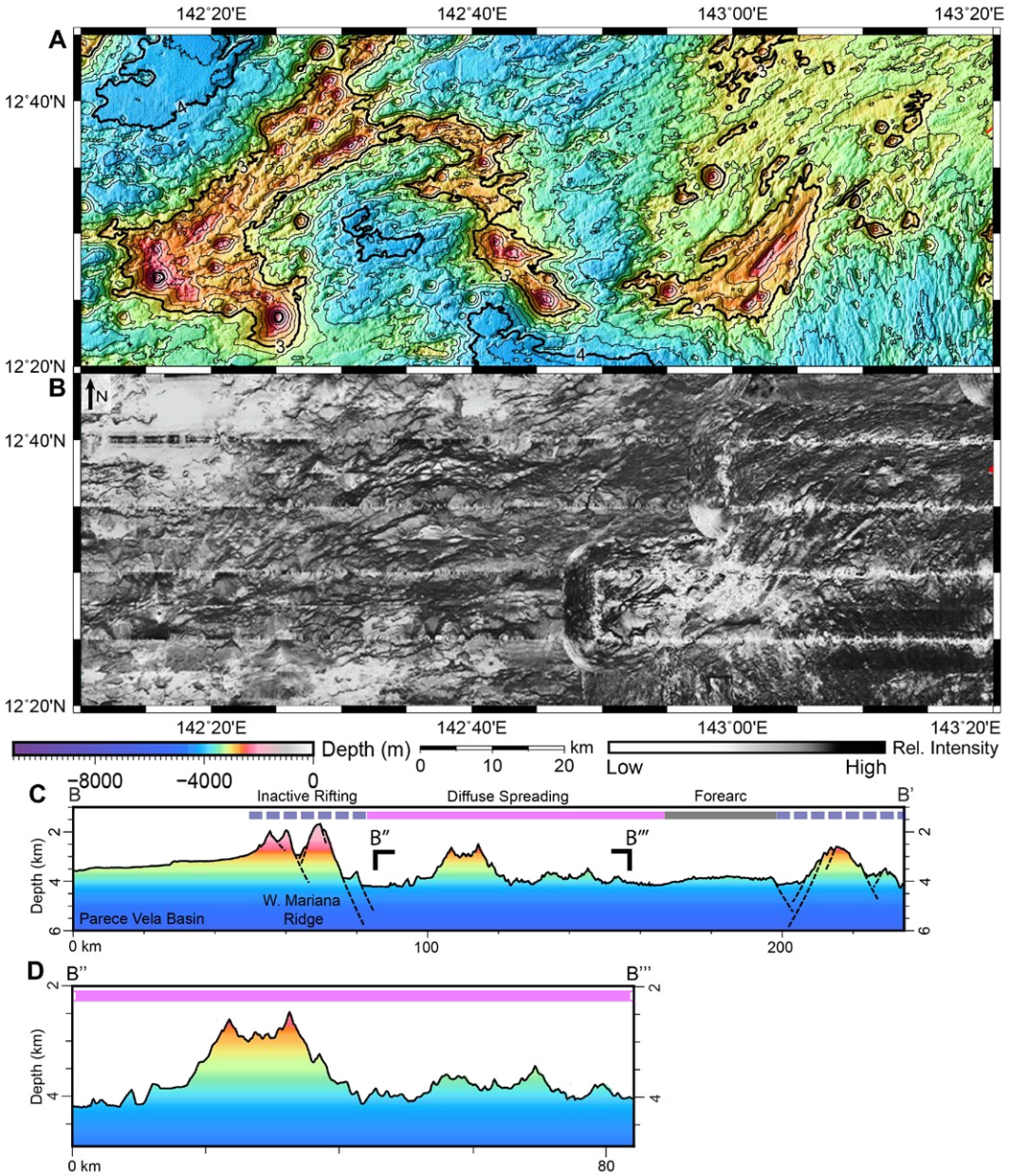


**Figure 8. Diffuse spreading zone (DSZ) focus area; see Figure 5 for regional context. (A) Compiled bathymetry map (0.0003° cell size, ~30 m) showing diffuse spreading zone morphology within the inferred active portion. Contour interval = 0.2 km (200 m); contour lines are bold and labeled every 1 km. (B) Compiled acoustic backscatter imagery (0.001° cell size, ~100 m). (C) B-B′: Cross section through the diffuse spreading zone, showing the inactive rift fabric of the West Mariana Ridge (WMR) transitioning abruptly into diffuse spreading fabric. The cross section (~7× vertical exaggeration) intersects the sedimented basin adjacent to the West Mariana Ridge, along with the NW pseudo-segment (described in section on "Malaguana-Gadao Ridge Spreading Morphology" and discussed in "Possible Diffuse Spreading Mechanisms" section) and a deep within the active zone. (D) B″-B‴: Close-up of a portion of B-B′ to show the volcanic terrain in more detail. Cross section location is shown on Figures 2 and 5A. See section of text on "Diffuse Spreading Zone Morphology" for detailed description.**

western end of the Malaguana-Gadao Ridge at 143°20′E (green zone in Fig. 3), and the inferred active portion of the diffuse spreading zone corresponds to the ~120-km-long by ~20–40-km-wide zone (red dashed area in Figs. 3, 4, 5, and 8B) with high backscatter (Figs. 5C and 8B) and distributed earthquakes (Fig. 7B) in the southern portion of the diffuse spreading zone. East of ~142°E, where the margins diverge, the deep grabens, kilometer-scale normal faults, and down-dropped crustal blocks characteristic of the Southwest Mariana Rift are no longer observed outside of the narrow relict rift zone (blue stripes in Fig. 3) along the West Mariana Ridge. The seafloor in the diffuse spreading zone has lower relief than the Southwest Mariana Rift, and the deepest portions of the diffuse spreading zone are ~1000 m shallower than the bottom of the Southwest Mariana Rift. Fault scarps in the diffuse spreading zone reach a maximum height of ~500 m, i.e., much smaller than the normal faults bounding the Southwest Mariana Rift graben. Cross-section B-B′ (Fig. 8C) intersects the relict rift fabric along the West Mariana Ridge and crosses the diffuse spreading fabric in the backarc (see Fig. 8D for detail), showing the contrasts in seafloor depth and relief.

The bathymetric map in Figure 8A shows the variety of morphologies in the diffuse spreading zone terrain, extending northward to the relict rift fabric along the West Mariana Ridge. In places, the volcanic cones form clusters of larger edifices, creating irregular patches of shallower average depth (outlined in black in Figs. 7A and 7B), while the deeper areas have fewer and smaller volcanic cones. North of ~12°35′N–12°40′N, the deeper areas are sedimented, burying any small volcanic features that may exist (Fig. 8B). The volcanic features in the diffuse spreading zone span a morphologic continuum in aspect ratio, from nearly circular cones to elongate cones with rift zones aligned with the local fabric, to linear ridges that shoal toward the center. The cones vary in diameter from a few hundred meters to nearly 10 km, with summit depths that vary from ~3500 m to as shallow as ~1800 m. The larger conical features with diameters greater than ~1–2 km are outlined on Figure 5B to highlight their distribution, along with both the volcanic lineations, defined by the ridge crests and rift zones extending away from some of the more elongate edifices, and tectonic lineations (consisting of normal fault scarps). The volcanic ridges are not continuous; they vary in length from a few kilometers up to ~20 km, and there is no clear segmentation pattern. Also, the seafloor on either side of the ridges is at a similar depth, and the ridges themselves have approximately symmetric slopes on both sides (Fig. 8D), indicating primarily volcanic and not tectonic origin. Many of the deeps, particularly in the western half of the diffuse spreading zone, are bounded by a fault scarp on at least one side, but many are simply topographic lows between two high-standing volcanic ridges, hence the use of "deep" as opposed to "graben" to describe these features.

West of 142°50′E, depths are more variable, with rougher topography and relief up to 2000 m between the high-standing volcanic features and the surrounding deeps, which average ~4000 m in depth. Volcanic cones are also more abundant compared to the eastern half (Figs. 5B and 8A) and have shallower summits, with 17 cones shallower than 2500 m, compared to only three in the eastern half. The eastern half is shallower than the western half overall (Fig. 8A), with the deepest seafloor near the edges reaching ~3600 m, and most of the seafloor surrounding the volcanic constructions varying between ~3000 and 3400 m. The volcanic features also have lower relief of a few hundred meters up to ~1200 m along the shallow volcanic ridge located at ~12°27′N, 143°05′E, giving the seafloor a smoother appearance than the western half.

The side-scan sonar imagery of the diffuse spreading zone (Fig. 8B; regional context is shown in Fig. 5C) shows a broad zone of high acoustic backscatter that is over 50 km wide near the Malaguana-Gadao Ridge terminus, tapering westward until it grades into the lower backscatter in the rift valley just west of 142°E. The much lower backscatter and subdued topography in the northern portion of the diffuse spreading zone (north of ~12°35′N–12°40′N; Fig. 5C) are consistent with pelagic sediment cover, suggesting that the high-backscatter part of the diffuse spreading zone was more recently active. HMR-1 shallow-towed side-scan imagery, described in detail in Becker (2005), shows that the high backscatter is related to a combination of effusive volcanism, with high-backscatter surfaces and lobate margins, and pervasive faulting throughout the region, although most of the faults are too small to resolve in the bathymetry data. The crescent-shaped ridge near 143°E, 12°25′N, along with the other large cones toward the west ("Unnamed" volcanoes mapped in Fig. 2), has low-backscatter terrain surrounded by higher-backscatter terrain (Fig. 8B), suggesting a locally derived source for the low-backscatter material. Given the high lava water contents measured in this area, the low backscatter is likely due to volcaniclastic material from particularly volatile-rich eruptions, such as that described from even deeper sections near the outer forearc (Stern et al., 2014), or at West Mata Volcano in the Lau Basin (Resing et al., 2011). None of the rock samples collected (shown in Fig. 4 and discussed in section on "Volcanism in the Southern Mariana Region") has been dated, so we do not have direct knowledge of how recent igneous activity may be, but the sample descriptions (Masuda, 2006) and available analyses (Becker, 2005; Pearce et al., 2005; Brounce et al., 2014) are consistent with relatively recent activity throughout the diffuse spreading zone high-backscatter zone.

The volcanic features were constructed on terrain consisting of shallower areas that include some larger cones and ridges (outlined in black on Figs. 7A and 7B) separated by bathymetric lows with similar but lower-relief features. The shallow volcanic zones are associated with mantle Bouguer anomaly lows, which in turn suggest thicker crust to compensate for the shallow seafloor, and the surrounding deeps are associated with relatively high mantle Bouguer anomaly values, indicating thinner crust. Thus, overall mantle Bouguer anomaly variations are qualitatively consistent with seafloor topography in local isostatic equilibrium. Within the western zone, there is a prominent ridge ~10 km wide and ~50 km long trending in a NE-SW direction and dotted with volcanic cones (marked with a thick dashed line on Fig. 7B) that we refer to as a "pseudo-segment." Mantle Bouguer anomalies within this zone vary between –10 mGal around the edges to as low as –50 mGal under the cluster of cones near the SW end of the pseudo-segment. Within the eastern zone, mantle Bouguer anomaly values are more uniform, consistent with the lower seafloor relief, varying between –10 and –25 mGal. A second pseudo-segment here (marked with a thick dashed line on Fig. 7B) is poorly defined and is dominated by a crescent-shaped

ridge. This ridge terminates at ~143°07′E, and there is a gap of ~20 km between the ridge and the Malaguana-Gadao Ridge terminus to the northeast, within which there is no clear continuation of this feature. Mantle Bouguer anomalies in the shallow zones are comparable to the Malaguana-Gadao Ridge near-axis crust (–20 to –50 mGal; light blue in Fig. 7A), and mantle Bouguer anomalies in the bathymetric lows (–5 to –20 mGal; green in Fig. 7A) are comparable to the distal Malaguana-Gadao Ridge flanks. This is consistent with a similar range in crustal thickness and density between the Malaguana-Gadao Ridge and diffuse spreading zone, in contrast to the lower mantle Bouguer anomaly values associated with the Southwest Mariana Rift and its flanks (–45 to –130 mGal).

## Malaguana-Gadao Ridge Spreading Morphology

Malaguana-Gadao Ridge axial morphology (Fig. 9) is characterized by a broad, rounded, axial high ~5 km wide and up to ~500–600 m above the surrounding seafloor (Martinez et al., 2000). The axial high has narrow, low-relief fissures visible in the IMI-30 side-scan imagery (Fig. 10A), but any topographic offsets associated with these are below the resolution of the ship multibeam bathymetry. Farther off axis, the ridge flanks are cut by axis-parallel normal faults with throws of up to ~200 m, ranging in length from ~10 to 50 km, resulting in seafloor fabric (Fig. 9A) that resembles abyssal hills on the flanks of

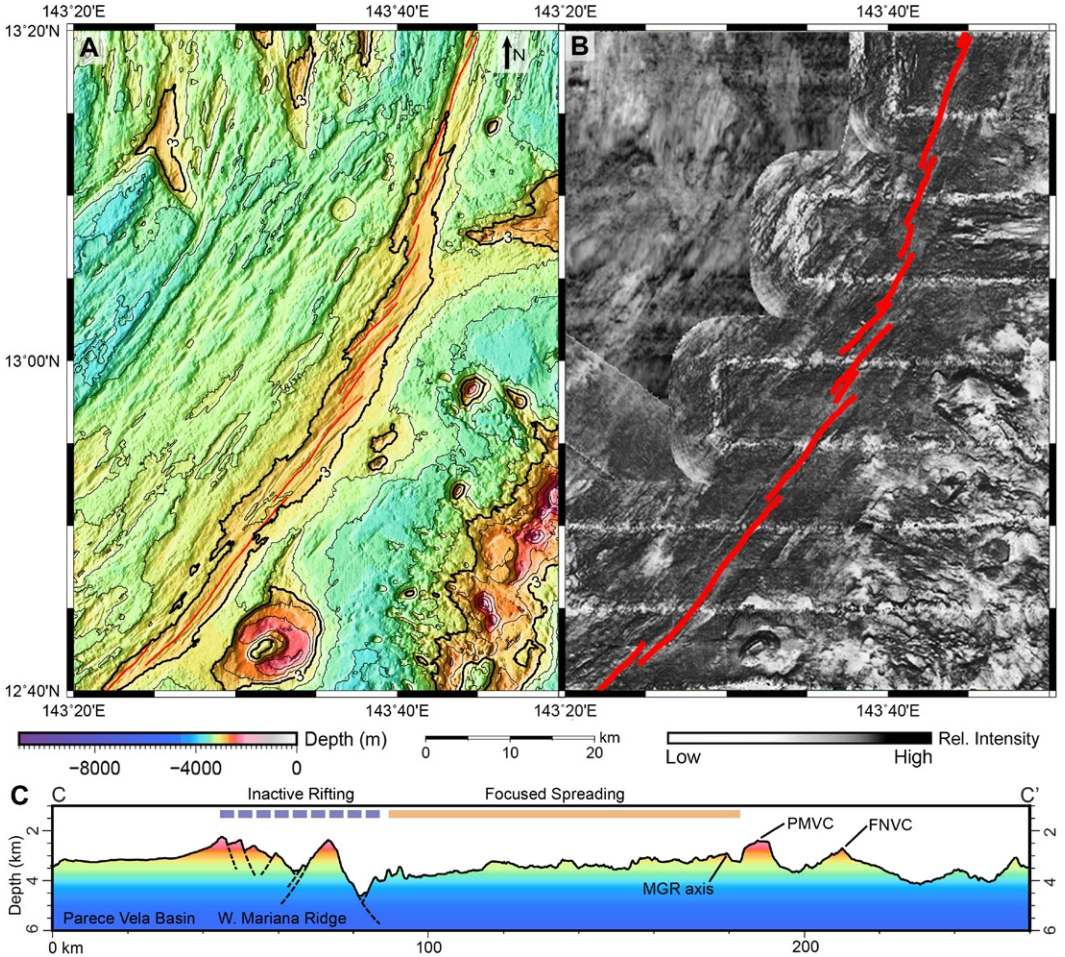


**Figure 9. Malaguano-Gadao Ridge (MGR) focus area; see Figure 5 for regional context. (A) Compiled bathymetry map (0.0003° cell size, ~30 m) showing focused spreading morphology on the Malaguana-Gadao Ridge flanks. Contour interval = 0.2 km (200 m); contour lines are bold and labeled every 1 km. Spreading axis is mapped in red on A and B. (B) Compiled acoustic backscatter imagery (0.001° cell size, ~100 m) of the Malaguana-Gadao Ridge. (C) C-C′: Cross section (~7× vertical exaggeration) across the Malaguana-Gadao Ridge (MGR) flanks, showing West Mariana Ridge rift fabric abruptly transitioning into abyssal hill–type fabric on the NW flank of the Malaguana-Gadao Ridge, and also intersecting the Patgon-Masala (PMVC) and Fina Nagu volcanic chains (FNVC) on the SE flank of the Malaguana-Gadao Ridge. Cross section location is shown on Figures 2 and 5A. See section of text on "Malaguana-Gadao Ridge Spreading Morphology" for detailed description.**

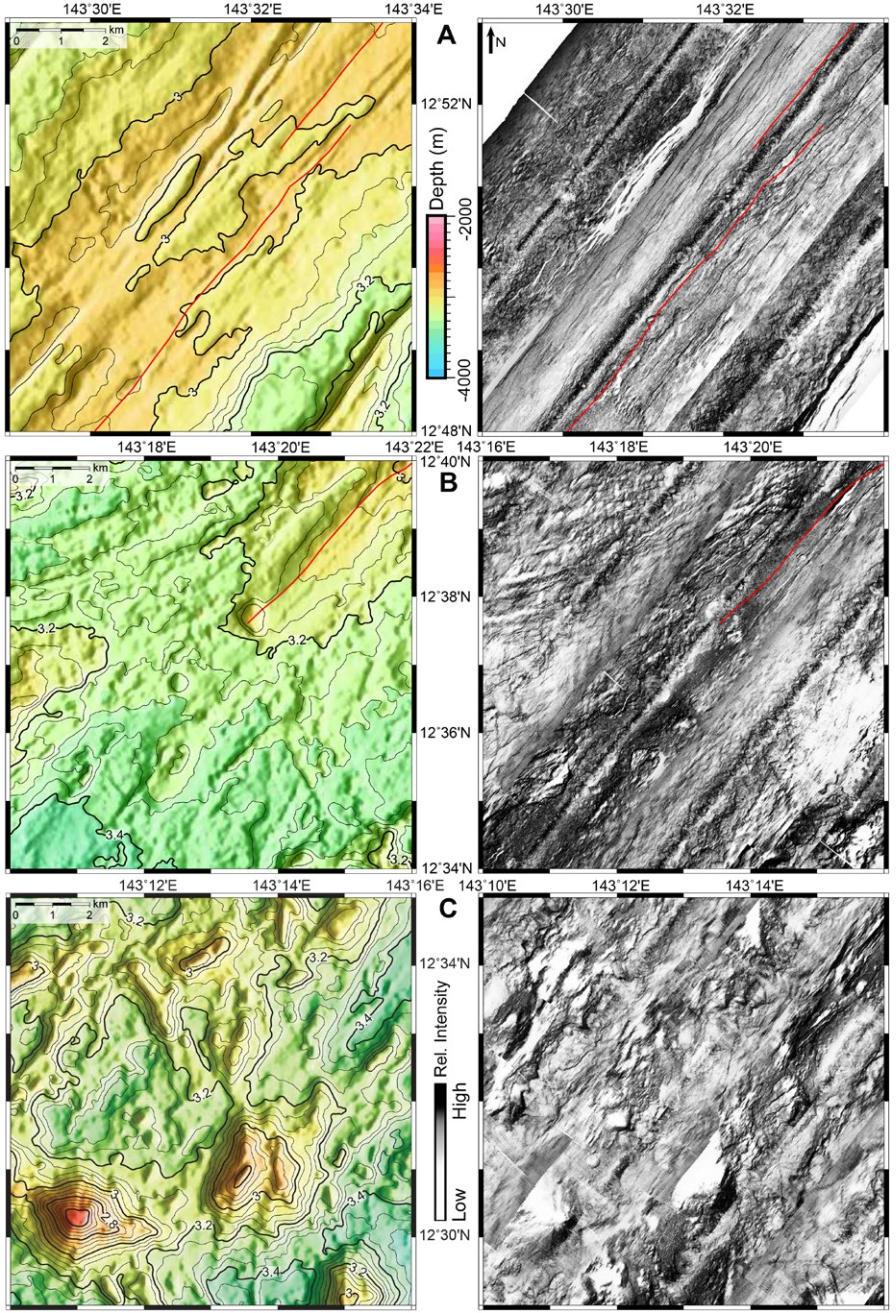


**Figure 10. Samples of fine-scale bathymetry (0.0001° cell size, ~10 m) on the left side (contour interval = 0.05 km [50 m], with bold and label every 0.2 km [200 m]), and IMI-30 backscatter imagery (0.00003° cell size, ~3 m) on the right side. (A) Malaguana-Gadao Ridge axial morphology. Note the broad rounded axial high with small normal faults and a third-order segment offset. The backscatter data show fine-scale axis-parallel fissures and faults that are too small to resolve in the bathymetric data, along with hummocky volcanic textures on the axial flanks. Spreading axis is marked with a thin red line in A and B. (B) Southern terminus of the Malaguana-Gadao Ridge axis. Note the abrupt end to the axial ridge and the abrupt change in morphology from a rounded volcanic axial high to a field of small volcanic mounds with faults that are no longer subparallel to the axis. (C) Fine-scale volcanic morphology in the eastern portion of the diffuse spreading zone. Note the mixture of morphologies in the bathymetry plot, and the mixture of high-backscatter and mottled backscatter volcanic textures in the IMI-30 backscatter data, possibly indicating a mixture of volcaniclastics and effusive hummocky lava flows.**

a fast-spreading mid-ocean ridge (Martinez et al., 2000), and this is the type example of focused seafloor spreading fabric (orange zone in Fig. 3).

There is a strong asymmetry in the fabric, with nearly all abyssal hill–type crust on the northwest flank of the Malaguana-Gadao Ridge (Fig. 9A). It is difficult to assess the degree of asymmetry in crustal accretion because the southeast flank of the Malaguana-Gadao Ridge is affected by faulting at high angles to the spreading axis and an absence of magnetic lineations (Martinez et al., 2018). Along the distal edges of the northwest flank, there is an abrupt transition between the abyssal hill fabric indicative of seafloor spreading and the relict block-faulted rifting fabric bordering the West Mariana Ridge (Figs. 2, 5A, and 9C), indicating a distinct phase of tectonic rifting rapidly transitioning to focused magmatic seafloor spreading. Typically, local sedimented deeps form between the base of the block-faulted West Mariana Ridge escarpment and the spreading fabric (Fig. 5C), suggesting that the final phase of arc rifting or the initial magmatic phase produced a short interval of thinner crust compared to later magmatic crustal accretion. The northwest flank of the Malaguana-Gadao Ridge also lacks the small volcanic cones that typify the diffuse spreading zone, with the morphology dominated by abyssal hill–like structures (Fig. 9A). The southeast flank hosts a series of larger volcanoes and calderas (Fig. 9A), including the Patgon-Masala volcanic chain adjacent to the Malaguana-Gadao Ridge (Masuda and Fryer, 2015) and the Fina Nagu volcanic chain (Brounce et al., 2016), which represent former or immature arc volcanic front edifices.

To highlight the differences and abrupt transition between focused spreading along the Malaguana-Gadao Ridge and the diffuse spreading zone fabric, we show maps of finely gridded multibeam bathymetry alongside IMI-30 backscatter imagery (Fig. 10). The smooth, rounded high of the Malaguana-Gadao Ridge axis (Fig. 10A) is cut by small fissures and a few normal faults with apparent throws up to ~150 m that are all subparallel to the axis. The western termination of the Malaguana-Gadao Ridge axis (Fig. 10B) is abrupt and marks the boundary between axis-parallel spreading fabric and the variable fabric of the diffuse spreading zone (Fig. 10C). Figure 10C shows typical diffuse spreading zone morphology, characterized by a mix of volcanic cones, short ridges, and smaller volcanic mounds covering the seafloor.

The mantle Bouguer anomaly (Fig. 7A) varies little along the Malaguana-Gadao Ridge and across its flanks, with values of ~–20 to –30 mGal near the axis increasing to as high as –10 mGal within the older seafloor northwest of the axis. There is a strong gradient between the negative anomalies (blues and greens) in the backarc and the positive anomalies associated with the thin forearc crust and the underlying subducting slab.

## Seismicity in the Southern Mariana Trough

Seismicity in the southern Mariana Trough (Fig. 7B) varies among the three regions described above and correlates with our morphologic observations. Shallow earthquakes (≤51 km depth) with $m_b$ ≥4 from the ISC reviewed bulletin (International Seismological Centre, 2020) are plotted as solid circles and scaled by their magnitudes, and focal mechanisms from the Global Centroid Moment Tensor Project (CMT) Catalog (Dziewonski et al., 1981; Ekström et al., 2012) are shown with "beachball" symbols (Fig. 7B). From a qualitative perspective, earthquakes within the Southwest Mariana Rift are more abundant and larger in magnitude compared to those in the diffuse spreading zone. Furthermore, the teleseismic earthquakes from the CMT catalog are almost exclusively limited to the Southwest Mariana Rift. Almost all of these show approximately NNW-SSE tension axes, approximately orthogonal to the trend of the rift. There is an abrupt decrease in the magnitude and number of events between ~142°E and 142°10′E near the transition from the Southwest Mariana Rift to the diffuse spreading zone, and minimal seismicity associated with the northwest pseudo-segment. Events between ~142°30′E and 143°E form a cluster of increased seismicity in the central portion of the diffuse spreading zone between the two pseudo-segments, and then seismicity decreases again from 143°E to the Malaguana-Gadao Ridge. Additionally, the width of the seismically active part of the diffuse spreading zone (Fig. 7B) closely matches that of the high-backscatter zone (Fig. 5C), consistent with a broad zone of relatively recent volcanic and tectonic activity. There is no distinct seismicity associated with the Malaguana-Gadao Ridge axis itself, with only a few small events scattered throughout the northwest flank, although seismicity increases dramatically to the southeast in the forearc due to the separate trench-parallel component of extension there (Martinez et al., 2018).

In order to quantify the contrasts between Southwest Mariana Rift and diffuse spreading zone seismicity, we selected the ISC events in the Southwest Mariana Rift (dark blue circles on Fig. 7B) and those within the inferred recently active portion of the diffuse spreading zone (purple circles on Fig. 7B), counted the number of events in each region, and then calculated the total moment release. In terms of total number of events (since 1962, and including one well-located event from 1935), the Southwest Mariana Rift has 406 versus 234 in the diffuse spreading zone, and because the regions are similar in size, we did not normalized the number of events per unit area. The maximum magnitude recorded within the Southwest Mariana Rift is $m_b$ 6.7 (large striped circle on the northern flank of the Southwest Mariana Rift in Fig. 7B), and the maximum within the diffuse spreading zone is $m_b$ 5.7. Along the Malaguana-Gadao Ridge and its northwest flank, the few scattered earthquakes are all less than $m_b$ 5. The total moment release in the Southwest Mariana Rift is ~6.5 times greater than that in the diffuse spreading zone, indicating more tectonic extension in the Southwest Mariana Rift and more magmatic extension in the diffuse spreading zone. This is consistent with the morphologic observations showing the prevalence of volcanic morphology in the diffuse spreading zone and tectonic rift morphology in the Southwest Mariana Rift. This is also analogous to observations from mid-ocean ridges as a function of spreading rate (Solomon et al., 1988) and magma budget (Buck et al., 2005), where an increasing proportion of extension is taken up tectonically as spreading rate decreases.

## DISCUSSION

The along-strike juxtaposition of three different modes of opening along the southern Mariana divergent boundary allows us to characterize a distinct mode of crustal accretion that we refer to as diffuse spreading, which occurs in an ~20–40-km-wide zone within the diffuse spreading zone. Based on clear contrasts in seafloor morphology and seismicity, diffuse spreading is distinct from rifting, or the tectonic stretching of preexisting lithosphere, which occurs within the Southwest Mariana Rift. It is also differentiated from focused seafloor spreading because crustal accretion occurs in a distributed manner over a broad region rather than focused along a narrow axis, such as that observed along the Malaguana-Gadao Ridge. To show this, we summarize observations of rifting and spreading in the southern Mariana Trough and then discuss possibly analogous regions in other backarc basins and consider potential mechanisms of accomplishing diffuse spreading. Finally, we present a conceptual model to explain how the combination of slow opening rates and high slab-fluid flux may create a broad zone of weak hydrous lithosphere, enabling the diffuse spreading process.

### Modes of Opening in the Southern Mariana Trough

Contrasts in seafloor morphology and seismicity between the Southwest Mariana Rift, the diffuse spreading zone, and the Malaguana-Gadao Ridge flanks provide strong evidence that each zone is controlled by different extensional processes. The Southwest Mariana Rift is characterized by tectonic rift–type morphology, with a deep, largely amagmatic rift valley bounded by normal faults with scarp heights up to 3500 m that progressively down-drop basement blocks to the valley floor. Abundant seismicity and normal fault focal mechanisms (Fig. 7B) indicate ongoing tectonic extension as a primary mode of opening. Relict rift fabric extends northeast in a narrow band along the eastern flank of the West Mariana Ridge (Fig. 3), indicating that a similar rifting process characterized the first phase of Mariana Trough opening.

East of the Southwest Mariana Rift, the morphology in the diffuse spreading zone changes abruptly. Diffuse spreading zone morphology is characterized by a mix of closely spaced volcanic cones and ridges superimposed on broader deeps and highs separated by gradational topographic transitions, rather than by large offset fault blocks. The characteristic features of large-scale tectonic rifting, such as fault block formation, are not observed in the diffuse spreading zone. The topographic ridges are much smaller and more closely spaced and appear to be largely volcanic, based on their bilaterally symmetric morphology. No evidence of fault blocks is observed in the bathymetry or gravity data, and the seismically active zone is associated with high acoustic backscatter that indicates relatively recent tectonic and volcanic activity. Seismicity decreases markedly within the diffuse spreading zone (Fig. 7B) compared to the Southwest Mariana Rift, both in terms of abundance and total moment release, consistent with a thinner brittle lithosphere (Solomon et al., 1988) and increasing magmatic accommodation of extension (Buck et al., 2005). Thinner brittle lithosphere under the diffuse spreading zone is also implied by earthquake depths recorded on a local ocean-bottom seismometer array across the Southwest Mariana Rift (Zhu et al., 2019), which showed that Southwest Mariana Rift earthquakes are both more abundant and deeper than those in the diffuse spreading zone, with maximum depths up to ~80 km for the Southwest Mariana Rift compared to <20 km for the diffuse spreading zone. Furthermore, seafloor depth in the diffuse spreading zone is distinctly shallower than in the Southwest Mariana Rift and the troughs that typically border the eastern flank of the West Mariana Ridge, but it is similar in average depth to the crust spread on the northwest flank of the Malaguana-Gadao Ridge. Apparently older, sedimented, and presumably relict diffuse spreading zone fabric extends northward from the edge of the inferred active zone (outlined with a thin red dashed line in Figs. 3, 4, 5, and 7B) to the narrow rifted margin of the West Mariana Ridge, indicating a short rifting phase that abruptly transitioned into diffuse spreading that remains active today. The development of diffuse spreading fabric from soon after the rift stage and its continuation to the present suggest that it is not a transitional phase between rifting and spreading, but rather a stable mode of extension that persists under appropriate conditions. This assertion is supported by the observation that there is no evidence of a diffuse spreading zone terrain flanking the Malaguana-Gadao Ridge, as would exist if diffuse spreading transitioned to focused spreading. Rather, Malaguana-Gadao Ridge abyssal hill fabric also extends to the West Mariana Ridge, indicating that each mode of crustal accretion began soon after rifting and persisted to the present. That is not to say that one mode cannot change into the other. Clearly, tectonic rifting preceded diffuse or focused spreading, and diffuse spreading may convert into focused spreading or vice versa depending on factors such as opening rate and slab dewatering rate, which may be influenced by other parameters such as subduction rate and slab age.

In contrast to the diffuse spreading zone, Malaguana-Gadao Ridge flank morphology is characterized by more uniform depths with abyssal hill–type fabric (Fig. 9A), although a long-wavelength deepening away from the axis toward the West Mariana Ridge is evident, consistent with thermal subsidence (Fig. 9C). As noted above, like the diffuse spreading zone fabric, characteristic Malaguana-Gadao Ridge flank seafloor spreading fabric extends to the narrow band of rift fabric (blue striped area in Fig. 3) along the West Mariana Ridge, indicating that rifting here rapidly transitioned to focused seafloor spreading, which remains active today. Along most of the eastern margin of the West Mariana Ridge the seafloor is locally deeper, isostatically indicating thinner rifted crust, before the transition to spreading takes place, and magmatic accretion causes the crust to thicken and shallow. A rapid transition from rifting to focused spreading appears to be typical in backarc basins, as is observed along most of the West Mariana Ridge (Fryer and Hussong, 1981; Yamazaki et al., 2003; Oakley et al., 2009), and along the rifted edges of the Kyushu-Palau Ridge abutting the Parece Vela and Shikoku Basins (Okino et al., 1994, 1998) (Fig. 1).

## Alternative Hypothesis: Diffuse Spreading versus Distributed Rifting

We interpret the diffuse spreading zone as a zone of distributed magmatic crustal accretion where new crust is emplaced in a broad region ~20–40 km wide. This newly created crust is also subject to tectonic extension, similar to crust within the plate-boundary zones at mid-ocean ridges (Macdonald, 1982). Thus, all the diffusely spread crust is distinct from and postdates the rifted arc crust, which is limited to narrow margins surrounding the West Mariana Ridge remnant arc and the conjugate edge of the Mariana forearc ridge.

In contrast, other models have proposed that tectonic rifting of the original arc terrain continues over a prolonged period of time and spatially forms much of the backarc basin. Such models imply that fragments of old arc crust (with ages predating the opening of the basin) should exist within the basin and form much of the basement, perhaps intruded and overlain by more recent lavas. Such models were applied, for example, to explain the evolution of the Lau Basin and Havre Trough, where a protracted rift phase was interpreted to form much of the western Lau Basin and most, if not all, of the Havre Trough before transitioning to focused seafloor spreading in parts of the Lau Basin (Parson and Hawkins, 1994; Hawkins, 1995a, 1995b; Parson and Wright, 1996; Wysoczanski et al., 2010). A similar rifting model has been suggested for the Mariana Trough north of 22°N (Yamazaki et al., 2003), and Martinez et al. (1995) had proposed a rifting and magmatic intrusion model for the 20°N–24°N area of the Mariana Trough. These models were primarily based on morphology, as old arc crust has never been found in the interior of the basins away from the rifted arc or remnant arc margins.

More recent studies have shown, however, that morphologically complex crust resembling the inferred rifted "basin and range" terrains of the western Lau Basin (Hawkins, 1995a, 1995b) can form in arc-proximal settings by magmatic seafloor spreading. At the Lau Basin Valu Fa Ridge, thick, irregular, felsic crust abruptly replaces thinner, uniform mafic crust as the ridge axis approaches the arc volcanic front (Martinez and Taylor, 2002; Dunn and Martinez, 2011). This transition is somewhat analogous to the change from the axial valley of the Mariana Trough spreading center to the axial high of the Malaguana-Gadao Ridge. However, like at the southern tip of the Malaguana-Gadao Ridge, another abrupt transition occurs at the southern end of the Valu Fa Ridge, along with decreasing spreading rates (~<40 mm/yr) (Sleeper and Martinez, 2016). Here, the prominent axial high of the Valu Fa Ridge is abruptly replaced by a "ridges and knolls" terrain (Fujiwara et al., 2001) comprising a broad zone of high acoustic backscatter characterized by positive seafloor magnetizations (Watanabe et al., 2010) and seafloor morphology similar to that observed in the diffuse spreading zone. Several of the "knolls" in this region have been sampled, and analyses have shown high volatile contents and strong arc-like signatures (Haase et al., 2009), also similar to the diffuse spreading zone. While previous studies (Parson and Hawkins, 1994; Parson and Wright, 1996; Fujiwara et al., 2001) had interpreted the area south of the Valu Fa Ridge as an arc rifting terrain, Martinez and Taylor (2006) hypothesized that this area, along with parts of the western Lau Basin, represented "diffuse patches of seafloor spreading" where spreading was not focused along a narrow axis. The prevalence of volcanic morphologies, high acoustic backscatter, and high magnetization values (Watanabe et al., 2010) are consistent with dominantly magmatic formation of this terrain within a broad zone of crustal accretion several tens of kilometers wide, similar to the diffuse spreading zone. Furthermore, we consider the continued stretching, rifting, and thinning of Lau arc crust ~200 km into the basin to the forearc Tonga Ridge as mechanically unlikely, especially given the abrupt thinning of the Lau and Tonga Ridges at their edges.

## Possible Diffuse Spreading Mechanisms

The observations presented herein support the interpretation of the diffuse spreading zone as a zone of distributed magmatic crustal accretion at least tens of kilometers wide, but precise limits on the width of the active zone and how activity is distributed, both spatially and temporally, are difficult to determine with current data. The similar ~20–40 km widths of both the zone of high backscatter and zone of seismicity support the interpretation that the entire zone is active, but more precise definition of this zone requires detailed near-bottom mapping and rock sampling, including determining radiometric ages. Fresh-looking glassy lava samples and the published analyses indicate recent volcanic activity within the diffuse spreading zone (Fig. 5B; Becker, 2005; Pearce et al., 2005; Masuda, 2006; Brounce et al., 2014), but the lack of radiometric ages on the samples makes it impossible to constrain the spatial and temporal distribution of volcanism.

The potentially analogous area south of the Valu Fa Ridge in the Lau Basin may provide some insight into the mechanism of diffuse spreading. There, distinct short (10–15-km-long) axes of higher magnetization have been observed within the overall positive magnetization area (Watanabe et al., 2010). These form en echelon and overlapping configurations and have been interpreted as fault-controlled intrusions and sites of localized volcanism. Their locally high magnetization may indicate the most recent sites of magmatic emplacement, as the magnetization of fresh volcanic rocks quickly attenuates with age (Johnson and Tivey, 1995). Thus, it is possible that the diffuse spreading process is accomplished through numerous short-lived but discrete dike intrusion and volcanic events along short axes that episodically relocate within the diffuse spreading zone. In addition, point source volcanic emplacements may also occur (Haase et al., 2009), forming the scattered small volcanic cones, but these do not appear to have a direct expression in sea-surface magnetization inversions (Watanabe et al., 2010). The active part of the zone may migrate laterally as the basin opens to remain near a peak in mantle wedge melting related to both hydrous fluxing from the slab and extensionally induced mantle upwelling and decompression melting.

Within the Mariana diffuse spreading zone, the pseudo-segments (thick dashed black lines in Fig. 7B) indicate that magmatism is not uniformly distributed and may provide some insight into the mechanism of diffuse spreading.

The nature of these features is difficult to determine with certainty utilizing the data presently available, but we will explore a few possibilities here. One possibility is that these features represent some degree of organization of spreading and may be roughly analogous to spreading segments separated by a nontransform offset. In this model, the cluster of seismicity between the pseudo-segments would then be related to largely strike-slip deformation in the offset zone, which is consistent with the strike-slip focal mechanism in the area (Fig. 7B). The morphology of the northwest pseudo-segment is broadly similar to a spreading segment (Becker, 2005), albeit with more volcanic cones, a more irregular shape, and a lack of abyssal hill fabric on the flanks. However, as described earlier, the southeast pseudo-segment is poorly defined in comparison, and there is an ~20 km gap between the crescent-shaped ridge that dominates most of the pseudo-segment and the tip of the Malaguana-Gadao Ridge axis, where the seafloor morphology is characterized by typical diffuse spreading zone ridges and knolls terrain (Figs. 7B and 8A). Thus, the morphology of the pseudo-segments is not consistent with focused axes of crustal accretion like the Malaguana-Gadao Ridge. Another possibility that is consistent with our hydrous lithosphere model (described in subsequent section titled "Hydrous Lithosphere Model") and the morphology is that the pseudo-segments are separate zones of diffuse spreading and represent the most recent loci of crustal accretion. The intervening cluster of seismicity could then be explained as a combination of strike-slip and extensional deformation in the offset zone. A third possibility that is also consistent with our hydrous lithosphere model is that extension is distributed relatively evenly throughout the diffuse spreading zone, and the topographic highs and lows may instead reflect local enhancements of melting or dynamic effects related to buoyant melt delivery within the overall zone of diffuse crustal accretion. In this model, the topographic highs are underlain by buoyant diapirs of hydrous melt, and the extension is locally accommodated almost entirely magmatically. This is consistent with the diminished seismicity along the pseudo-segments and other prominent volcanic features in the diffuse spreading zone, and the lack of abyssal hills. The cluster of seismicity between the pseudo-segments may then simply be a region that is not underlain by hydrous diapirs and thus has a lower magma supply and greater proportion of tectonic extension.

## Volcanism in the Diffuse Spreading Zone and Malaguana-Gadao Ridge: Melt Generation and Focusing Processes

The distribution and morphologic variety of volcanic features within the diffuse spreading zone imply local variability in both melt production and tectonic extension not evident at the Malaguana-Gadao Ridge, which accretes crust more uniformly along its narrow axis. These contrasts provide insight into the mechanisms of melt generation in the underlying mantle wedge and melt focusing and homogenization in the lithosphere.

Both the Malaguana-Gadao Ridge and the diffuse spreading zone overlie slab depths typically associated with arc volcanism, with sampled lavas showing strong affinities to arc-type magmas (Becker, 2005; Pearce et al., 2005; Brounce et al., 2014), and measured water contents ranging between ~1.5% and 2.5% (Brounce et al., 2014). The contrasts between these two regions thus cannot be explained simply by major differences in mantle wedge composition. Based on the abrupt nature of the transition between the Malaguana-Gadao Ridge and diffuse spreading zone morphologies, it appears that a rheologic threshold is reached. This threshold is probably controlled by a combination of slowing opening rates and mantle hydration, where the lithosphere becomes weak enough that extension changes from focused to diffuse spreading. Melt focusing effects that depend on deeper mantle viscosity (strongly affected by water content) have also been proposed (Phipps Morgan, 1997; Spiegelman and McKenzie, 1987), so the weakening due to hydration may also extend deeper into the mantle wedge. Thus, the morphologic differences between the diffuse spreading zone and the Malaguana-Gadao Ridge may reflect changes in lithospheric and mantle melt focusing mechanisms between these two systems, controlled by a rheological threshold.

One of the most striking contrasts between diffuse spreading zone morphology and the Malaguana-Gadao Ridge flanks is the numerous small seamounts throughout the diffuse spreading zone and the lack of such features on the Malaguana-Gadao Ridge flanks. Within the diffuse spreading zone, buoyant mantle upwelling instabilities (diapirs) that would normally form arc volcanoes may be entrained within the broad plate-driven mantle upwelling regime. With no stable spreading axis and associated subaxial magma lens within which to homogenize and differentiate, the diffuse spreading zone volcanic emplacements thus may more closely reflect primitive melts formed in the mantle wedge. The two lava samples from the eastern diffuse spreading zone analyzed by Brounce et al. (2014) are consistent with this interpretation, with higher average MgO content, lower average $SiO_2$ content, and higher average Ba/La and Sr/Nd ratios compared to the Malaguana-Gadao Ridge samples, indicating more mafic and primitive melts. Analyses of lavas from similar seamounts south of the Valu Fa Ridge in the Lau Basin also show more primitive and heterogeneous compositions compared to the Valu Fa Ridge (Haase et al., 2009), but more analyses on samples distributed throughout the diffuse spreading zone are necessary to confirm this.

The Malaguana-Gadao Ridge has melt-focusing mechanisms like those at oceanic mid-ocean ridges (e.g., Phipps Morgan, 1997) and possibly a continuous subaxial magma lens, as observed on one seismic reflection profile near 13°05′N (Becker et al., 2010). These features would help to homogenize mantle melts within the subaxial magmatic system of the Malaguana-Gadao Ridge so that they erupt at the linear axial summit trough as effusive flows rather than small melt batches forming individual cones. Without such homogenization mechanisms, the irregular shape of the shallow volcanic zones within the diffuse spreading zone may thus reflect the three-dimensional pattern of melt formation and buoyant upwelling in the mantle wedge. The smoother seafloor morphology of the Malaguana-Gadao Ridge reflects the mantle and lithospheric focusing mechanisms acting on similar arc volcanic front melts.

## Hydrous Lithosphere Model

The position of the diffuse spreading zone overlying slab depths with expected high water flux (Schmidt and Poli, 1998) suggests likely controls on this form of crustal accretion based on the effects of water on mantle rheology (Fig. 11; Hirth and Kohlstedt, 1996; Phipps Morgan, 1997). At mid-ocean ridges, the small amount of mantle water present is extracted into the melt, dehydrating and strongly increasing the viscosity of the residual mantle (Karato et al., 1986; Hirth and Kohlstedt, 1996). The up to 1000-fold increase in viscosity is hypothesized to produce a "compositional lithosphere" (Phipps Morgan, 1997) (see also Fig. 11A) that inhibits off-axis volcanism and is thought to help focus the melt from a broad ~200-km-wide zone of melt generation at depth toward a narrow neovolcanic zone at the surface (Spiegelman and McKenzie, 1987; Braun et al., 2000; Key et al., 2013).

In our hydrous lithosphere model (Fig. 11B; Martinez et al., 2012), the continuous flux of water from the slab beneath the diffuse spreading zone inhibits dehydration of the mantle wedge. This leads to increased hydration of the melt and residual mantle, which decreases the viscosity and produces a broad zone of weak hydrous lithosphere rather than strong compositional lithosphere. For simplicity, we assume that the rate of water addition from the slab is the same for the Malaguana-Gadao Ridge and diffuse spreading zone. This is likely controlled to first order by the rate of Pacific plate subduction, which is not significantly different between these settings (~27–28 mm/yr; Kato et al., 2003; see Fig. 1 herein). However, the rate of mantle flow through the melting regimes and the rates of mantle melting and crustal production are different. As opening rates slow westward (to very slow rifting rates at the Southwest Mariana Rift), the steady water flux from the slab is distributed within a decreasing volume of mantle flowing through the melting regime of the diffuse spreading zone compared with the Malaguana-Gadao Ridge. Therefore, since the rate of water addition is constant and the rate of water extraction is decreasing, the concentration of water in the mantle wedge should increase westward from the Malaguana-Gadao Ridge to the diffuse spreading zone, and thus both melts and residual mantle should have increasing water contents. At some point, the westward-increasing mantle water content leads to a low enough lithospheric strength that the lithosphere deforms diffusely in a broad zone. This appears to be a threshold effect, because the change in mode of crustal accretion is abrupt, transitioning at the southern tip of the Malaguana-Gadao Ridge from a focused narrow zone dominated by effusive sheet flows emanating from a narrow axis to distributed intrusions and dikes forming narrow volcanic ridges and scattered small volcanic cones. Once this threshold is reached, there appears to be a particular range of conditions wherein the rate of water input from the slab and the rate of mantle water extraction by plate-driven decompression melting maintain a weak mantle and lithosphere and allow diffuse spreading to continue. Other factors, such as plate cooling with age (Parsons and Sclater, 1977) and the fact that the rate of mantle upwelling

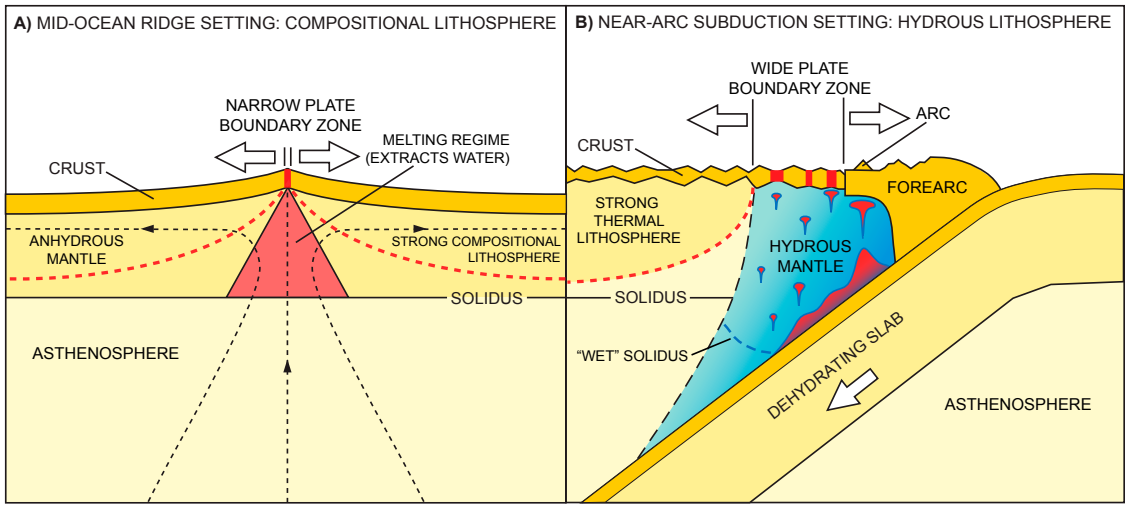


**Figure 11. (A) Simplified conceptual cross section (~1:1 scale) through a typical mid-ocean ridge, based on the compositional lithosphere model of Phipps Morgan (1997). Melting and melt extraction within the subridge melting regime dehydrate the upwelling mantle and create a dry and strong compositional lithosphere that helps to focus melt and deformation to a narrow plate-boundary zone. Black dashed lines with arrows show the generalized pattern of mantle flow. (B) Simplified conceptual depiction of the hydrous lithosphere model (modified from Martinez et al., 2012, 2018), showing a cross section (~1:1 scale) through a typical subduction zone with active near-arc extension analogous to the southern Mariana Trough diffuse spreading zone, though here the forearc massif is still intact. The dehydrating slab continually adds water to the overlying mantle wedge and lithosphere, so that even though mantle melting occurs, the residual mantle retains significant water (Hirth and Kohlstedt, 2003), and a strong compositional lithosphere cannot form. Deformation and volcanism cannot focus and are distributed in a broad plate-boundary zone. Thick red bars in the crust depict distributed volcanism, red dashed line shows the base of the thermal lithosphere, and red blob and diapirs schematically depict hydrous melt; other features are labeled. The blue gradient within the mantle wedge represents increasing mantle water content toward the arc, and the dashed black line marks the hypothesized sharp boundary between a strongly hydrous mantle wedge and less hydrous mantle away from the arc (Dunn and Martinez, 2011; Sleeper and Martinez, 2014). See section of text on "Hydrous Lithosphere Model" for discussion.**

varies inversely with the width of the zone undergoing extension (Buck et al., 1988), likely contribute to determining the width of the zone of active crustal accretion. This model is based on geophysical observations and general principles, but the current distribution of lava sample analyses is not sufficient to test the primary prediction that mantle wedge water content increases from the Malaguana-Gadao Ridge through the diffuse spreading zone. More lava sampling throughout the diffuse spreading zone and, in particular, systematic measurements of water content are necessary to test and confirm the model.

Another aspect of the model is a hypothesized abrupt boundary (dashed black line in Fig. 11B) between a strongly hydrous mantle wedge with increasing water content toward the arc volcanic front (shown with blue color gradient in Fig. 11B) and distinctly less hydrous mantle away from the arc. This hypothesis is based on abrupt changes in depth, morphology, crustal structure, thickness, and chemistry seen in the Lau Basin spreading centers with arc proximity (Dunn and Martinez, 2011; Martinez and Taylor, 2002; Escrig et al., 2009; Sleeper and Martinez, 2014; Sleeper et al., 2016). A similar transition in morphology and crustal structure is observed in the Mariana Trough near 14°22′N, where the crust thickens rapidly from ~3.4–4.1 km to ~5.9–6.9 km to the south, as inferred from multibeam mapping and gravity studies (Kitada et al., 2006). The change in crustal thickness is accompanied by a rapid change in morphology from an axial valley to an axial high, also similar to the Lau Basin. The association of abrupt crustal thickness changes with the position of the extension axis relative to the slab supports the inference that similar changes in mantle hydration occur in the Mariana mantle wedge (Fig. 11B) to those inferred in the Lau Basin (Sleeper and Martinez, 2014; Sleeper et al., 2016). However, an alternative hypothesis (rather than an abrupt change in mantle water content) is a more gradational variation in water content inducing a threshold effect on mantle rheology and strength. We posit a similar threshold effect to explain the abrupt change in mode of crustal accretion between the Malaguana-Gadao Ridge and diffuse spreading zone, and such threshold effects are observed in abrupt mid-ocean-ridge transitions from axial highs to axial valleys despite gradational changes in spreading rate, mantle temperature, or melt production. They are thought to be induced by rapid changes in near-axis lithospheric strength resulting from the presence or absence of a subaxial melt lens or other threshold changes in rheologic properties (Phipps Morgan and Chen, 1993; Ma and Cochran, 1996, 1997; Cochran and Sempere, 1997). As water content strongly affects both mantle melting and strength, it is possible that an abrupt threshold effect occurs even with gradual changes in mantle water content or opening rates, and this may explain the abrupt nature of the transition in morphology and crustal thickness along the Malaguana-Gadao Ridge as well as the abrupt change in mode of crustal accretion between the Malaguana-Gadao Ridge and diffuse spreading zone.

## CONCLUSIONS

This study describes three modes of opening along the southern Mariana divergent boundary and, in particular, a new mode of magmatic crustal accretion that we call diffuse spreading, where the zone of active crustal accretion is ~20–40 km wide, rather than 1–2 km wide as at mid-ocean ridges and typical backarc spreading centers. The diffuse spreading zone is an ~120-km-long region in the southern Mariana Trough between the southern terminus of the Malaguana-Gadao Ridge spreading center to the east and the active rift valley of the Southwest Mariana Rift to the west. Diffuse spreading zone seafloor morphology is characterized by small volcanic cones and closely spaced ridges superimposed on broader swells and deeps that is unlike the block faulting produced by rifting and is also unlike the abyssal hill fabric associated with focused spreading. Similar seafloor fabric has been identified in other backarc settings, although it has been interpreted as a form of tectonic arc rifting (Hawkins, 1995a, 1995b; Parson and Wright, 1996; Fujiwara et al., 2001; Yamazaki et al., 2003; Watanabe et al., 2010; Wysoczanski et al., 2010). In the southern Mariana Trough, however, the continuity of the divergent boundary and the nature of the flanking seafloor allow a side-by-side comparison to be made of the characteristics of the various modes of opening. These characteristics indicate that diffuse spreading is a distinct mode of magmatic crustal accretion that occurs within a broad zone of weak hydrous lithosphere, maintained by slow opening and a continuous flux of slab water. This slab hydrous fluxing counteracts the mantle dehydration and strengthening that normally accompany melting at mid-ocean ridges, weakening the lithosphere and creating a broad plate-boundary zone. Thus, diffuse spreading is likely restricted to supraslab settings of backarc basins, where extension occurs close to the arc volcanic front or within the forearc. Spreading rate also appears to be a controlling factor, as it determines the rate of mantle upwelling and melting, and thus the rate of water extraction from the mantle for a given water influx from the slab. Based on the abrupt change in seafloor morphology between the diffuse spreading zone and the abyssal hill fabric of the Malaguana-Gadao Ridge, the transition between focused and diffuse spreading appears to be a threshold phenomenon.

Diffuse spreading is not a transitional phase from rifting to focused spreading but appears to be a stable form of crustal accretion associated with particular mantle hydration and kinematic conditions. In addition to the diffuse spreading zone in the southern Mariana Trough, parts of the southern Lau Basin and Havre Trough as well as the Mariana Trough north of 22°N may represent further examples. More detailed geophysical mapping and analysis of volcanic rock samples from the southern Mariana Trough and other backarc basins are needed to elucidate the occurrence of and controls on diffuse spreading.

#### ACKNOWLEDGMENTS

This work was supported by National Science Foundation grants OCE-0961811 to Fernando Martinez, OCE-0961352 to Robert J. Stern, and OCE-0961559 to Katherine A. Kelley. Further support was provided through the Denise B. Evans Fellowship to J.D. Sleeper, administered by the Hawai'i Institute of Geophysics and Planetology at the University of Hawai'i at Mānoa. Underway geophysical data from R/V *Thomas G. Thompson* expedition TN273 are available at http://www.rvdata.us/catalog/TN273. We would also like to thank the captain and crew of R/V *Thomas G.*

*Thompson* and acknowledge the contributions of the Hawai'i Mapping Research Group team for their expertise in operating the IMI-30 deep-towed side-scan sonar system and initial onboard data processing. Lastly, we thank two anonymous reviewers for their thoughtful comments and suggestions to improve the manuscript. University of Hawai'i at Mānoa *School of Ocean and Earth Science and Technology* (SOEST) contribution #11335, Hawai'i Institute of Geophysics and Planetology (HIGP) contribution #2446, and University of Texas at Dallas (UTD) Geosciences contribution #1668.

## REFERENCES CITED

Amante, C., and Eakins, B.W., 2009, ETOPO1 Arc-Minute Global Relief Model: Procedures, Data Sources, and Analysis: National Oceanic and Atmospheric Administration (NOAA) Technical Memorandum NESDIS NGDC-24, National Geophysical Data Center, NOAA, https://doi.org/10.7289/V5C8276M (accessed 19 September 2020).

Arai, R., and Dunn, R.A., 2014, Seismological study of Lau back arc crust: Mantle water, magmatic differentiation, and a compositionally zoned basin: Earth and Planetary Science Letters, v. 390, p. 304–317, https://doi.org/10.1016/j.epsl.2014.01.014.

Armstrong, A.A., 2011, U.S. Extended Continental Shelf Cruise to Map Sections of the Mariana Trench and the Eastern and Southern Insular Margins of Guam and the Northern Mariana Islands: University of New Hampshire Center for Coastal and Ocean Mapping/Joint Hydrographic Center (UNH/CCOM-JHC) Cruise SU10–02, Leg 2, Apra, Guam: Durham, New Hampshire, University of New Hampshire, Center for Coastal and Ocean Mapping/Joint Hydrographic Center, 45 p.

Baker, E.T., Embley, R.W., Walker, S.L., Resing, J.A., Lupton, J.E., Nakamura, K.-i., de Ronde, C.E.J., and Massoth, G.J., 2008, Hydrothermal activity and volcano distribution along the Mariana arc: Journal of Geophysical Research–Solid Earth, v. 113, B08S09, https://doi.org/10.1029/2007jb005423.

Baker, N., Fryer, P., Martinez, F., and Yamazaki, T., 1996, Rifting history of the northern Mariana Trough: SeaMARC II and seismic reflection surveys: Journal of Geophysical Research–Solid Earth, v. 101, p. 11427–11455, https://doi.org/10.1029/95JB02853.

Becker, N.C., 2005, Recent Volcanic and Tectonic Evolution of the Southern Mariana Arc [Ph.D. thesis]: Honolulu, Hawai'i, University of Hawai'i at Mānoa, 187 p.

Becker, N.C., Fryer, P., and Moore, G.F., 2010, Malaguana-Gadao Ridge: Identification and implications of a magma chamber reflector in the southern Mariana Trough: Geochemistry Geophysics Geosystems, v. 11, Q04X13, https://doi.org/10.1029/2009GC002719.

Bird, P., 2003, An updated digital model of plate boundaries: Geochemistry Geophysics Geosystems, v. 4, no. 3, 1027, https://doi.org/10.1029/2001GC000252.

Bloomer, S.H., Stern, R.J., and Smoot, N.C., 1989, Physical volcanology of the submarine Mariana and Volcano arcs: Bulletin of Volcanology, v. 51, p. 210–224, https://doi.org/10.1007/BF01067957.

Braun, M.G., Hirth, G., and Parmentier, E.M., 2000, The effects of deep damp melting on mantle flow and melt generation beneath mid-ocean ridges: Earth and Planetary Science Letters, v. 176, no. 3–4, p. 339–356, https://doi.org/10.1016/S0012-821X(00)00015-7.

Brounce, M.N., Kelley, K.A., and Cottrell, E., 2014, Variations in $Fe^{3+}/\Sigma Fe$ of Mariana arc basalts and mantle wedge $fO_2$: Journal of Petrology, v. 55, no. 12, p. 2513–2536, https://doi.org/10.1093/petrology/egu065.

Brounce, M.N., Kelley, K.A., Stern, R.J., Martinez, F., and Cottrell, E., 2016, The Fina Nagu volcanic complex: Unusual submarine arc volcanism in the rapidly deforming southern Mariana margin: Geochemistry Geophysics Geosystems, v. 17, p. 4078–4091, https://doi.org/10.1002/2016GC006457.

Brune, S., Popov, A.A., and Sobolev, S.V., 2012, Modeling suggests that oblique extension facilitates rifting and continental break-up: Journal of Geophysical Research–Solid Earth, v. 117, B08402, https://doi.org/10.1029/2011JB008860.

Buck, W.R., Martinez, F., Steckler, M.S., and Cochran, J.R., 1988, Thermal consequences of lithospheric extension: Pure and simple: Tectonics, v. 7, no. 2, p. 213–234, https://doi.org/10.1029/TC007i002p00213.

Buck, W.R., Lavier, L.L., and Poliakov, A.N.B., 2005, Modes of faulting at mid-ocean ridges: Nature, v. 434, no. 7034, p. 719–723, https://doi.org/10.1038/nature03358.

Cochran, J.R., and Sempere, J.-C., 1997, The Southeast Indian Ridge between 88E and 118E: Gravity anomalies and crustal accretion at intermediate spreading rates: Journal of Geophysical Research–Solid Earth, v. 102, p. 15463–15487, https://doi.org/10.1029/97JB00511.

Dunn, R.A., and Martinez, F., 2011, Contrasting crustal production and rapid mantle transitions beneath backarc ridges: Nature, v. 469, p. 198–202, https://doi.org/10.1038/nature09690.

Dunn, R.A., Martinez, F., and Conder, J.A., 2013, Crustal construction and magma chamber properties along the Eastern Lau spreading center: Earth and Planetary Science Letters, v. 371–372, p. 112–124, https://doi.org/10.1016/j.epsl.2013.04.008.

Dziewonski, A.M., Chou, T.-A., and Woodhouse, J.H., 1981, Determination of earthquake source parameters from waveform data for studies of global and regional seismicity: Journal of Geophysical Research–Solid Earth, v. 86, p. 2825–2852, https://doi.org/10.1029/JB086iB04p02825.

Eason, D.E., and Dunn, R.A., 2015, Petrogenesis and structure of oceanic crust in the Lau backarc basin: Earth and Planetary Science Letters, v. 429, p. 128–138, https://doi.org/10.1016/j.epsl.2015.07.065.

Ekström, G., Nettles, M., and Dziewonski, A.M., 2012, The global CMT project: 2004–2010: Centroid-moment tensors for 13,017 earthquakes: Physics of the Earth and Planetary Interiors, v. 200–201, p. 1–9, https://doi.org/10.1016/j.pepi.2012.04.002.

Escrig, S., Bézos, A., Goldstein, S.L., Langmuir, C.H., and Michael, P.J., 2009, Mantle source variations beneath the Eastern Lau spreading center and the nature of subduction components in the Lau Basin Tonga arc system: Geochemistry Geophysics Geosystems, v. 10, Q04014, https://doi.org/10.1029/2008GC002281.

Fryer, P., 1995, Geology of the Mariana Trough, *in* Taylor, B., ed., Backarc Basins: Tectonics and Magmatism: New York, Plenum Press, p. 237–279.

Fryer, P., 1996, Evolution of the Mariana convergent plate margin system: Reviews of Geophysics, v. 34, p. 89–125, https://doi.org/10.1029/95RG03476.

Fryer, P., 2012, Serpentinite mud volcanism: Observations, processes, and implications: Annual Review of Marine Science, v. 4, p. 345–373, https://doi.org/10.1146/annurev-marine-120710-100922.

Fryer, P., and Hussong, D.M., 1981, Seafloor spreading in the Mariana Trough: Results of Leg 60 drill site selection surveys, *in* Hussong, D.M., et al., Initial Reports of the Deep Sea Drilling Project, Volume 60: Washington, D.C., U.S. Government Printing Office, p. 45–55.

Fryer, P., Ambos, E.L., and Hussong, D.M., 1985, Origin and emplacement of Mariana fore-arc seamounts: Geology, v. 13, no. 11, p. 774–777, https://doi.org/10.1130/0091-7613(1985)13<774:OAEOMF>2.0.CO;2.

Fryer, P., Fujimoto, H., Sekine, M., Johnson, L.E., Kasahara, J., Masuda, H., Gamo, T., Ishii, T., Ariyoshi, M., and Fujioka, K., 1998, Volcanoes of the southwestern extension of the active Mariana island arc: New swath-mapping and geochemical studies: The Island Arc, v. 7, p. 596–607, https://doi.org/10.1111/j.1440-1738.1998.00212.x.

Fryer, P., Becker, N.C., Applegate, B., Martinez, F., Edwards, M., and Fryer, G., 2003, Why is the Challenger Deep so deep?: Earth and Planetary Science Letters, v. 211, p. 259–269, https://doi.org/10.1016/S0012-821X(03)00202-4.

Fujiwara, T., Yamazaki, T., and Joshima, M., 2001, Bathymetry and magnetic anomalies in the Havre Trough and southern Lau Basin: From rifting to spreading in backarc basins: Earth and Planetary Science Letters, v. 185, p. 253–264, https://doi.org/10.1016/S0012-821X(00)00378-2.

Haase, K.M., Fretzdorff, S., Mühe, R., Garbe-Schönberg, D., and Stoffers, P., 2009, A geochemical study of off-axis seamount lavas at the Valu Fa Ridge: Constraints on magma genesis and slab contributions in the southern Tonga subduction zone: Lithos, v. 112, p. 137–148, https://doi.org/10.1016/j.lithos.2009.05.041.

Hawkins, J.W., 1995a, The geology of the Lau Basin, *in* Taylor, B., ed., Backarc Basins: Tectonics and Magmatism: New York, Plenum Press, p. 63–138, https://doi.org/10.1007/978-1-4615-1843-3_3.

Hawkins, J.W., 1995b, Evolution of the Lau Basin—Insights from ODP Leg 135, *in* Hawkins, J.W., et al., Proceedings of the Ocean Drilling Program Leg 135, Scientific Results: College Station, Texas, Ocean Drilling Program, p. 879–905.

Hayes, G.P., Moore, G.L., Portner, D.E., Hearne, M., Flamme, H., Furtney, M., and Smoczyk, G.M., 2018, Slab2, a comprehensive subduction zone geometry model: Science, v. 362, no. 6410, p. 58–61, https://doi.org/10.1126/science.aat4723.

Hirth, G., and Kohlstedt, D.L., 1996, Water in the oceanic upper mantle: Implication for rheology, melt extraction, and the evolution of the lithosphere: Earth and Planetary Science Letters, v. 144, p. 93–108, https://doi.org/10.1016/0012-821X(96)00154-9.

Hirth, G., and Kohlstedt, D., 2003, Rheology of the upper mantle and the mantle wedge: A view from the experimentalists, *in* Eiler, J., ed., Inside the Subduction Factory: American Geophysical Union Geophysical Monograph 138, p. 83–105, https://doi.org/10.1029/138GM06.

Hussong, D.M., and Uyeda, S., 1981, Tectonic processes and the history of the Mariana arc: A synthesis of the results of Deep Sea Drilling Project Leg 60, *in* Hussong, D.M., et al., Initial

Reports of the Deep Sea Drilling Project, Volume 60: Washington, D.C., U.S. Government Printing Office, p. 909–929.
International Seismological Centre, 2020, On-line Bulletin: http://doi.org/10.31905/D808B830 (accessed 23 July 2020).
Johnson, H.P., and Tivey, M.A., 1995, Magnetic properties of zero-age oceanic crust: A new submarine lava flow on the Juan de Fuca Ridge: Geophysical Research Letters, v. 22, no. 2, p. 175–178, https://doi.org/10.1029/94GL02053.
Kanamori, H., 1977, The energy release in great earthquakes: Journal of Geophysical Research, v. 82, p. 2981–2987, https://doi.org/10.1029/JB082i020p02981.
Karato, S.-I., Paterson, M., and Fitzgerald, J., 1986, Rheology of synthetic olivine aggregates: Influence of grain size and water: Journal of Geophysical Research, v. 91, p. 8151–8176, https://doi.org/10.1029/JB091iB08p08151.
Karig, D.E., 1971, Structural history of the Mariana island arc system: Geological Society of America Bulletin, v. 82, p. 323–344, https://doi.org/10.1130/0016-7606(1971)82[323:SHOTMI]2.0.CO;2.
Karig, D.E., 1972, Remnant arcs: Geological Society of America Bulletin, v. 83, p. 1057–1068, https://doi.org/10.1130/0016-7606(1972)83[1057:RA]2.0.CO;2.
Karig, D.E., Anderson, R.N., and Bibee, L.D., 1978, Characteristics of back arc spreading in the Mariana Trough: Journal of Geophysical Research–Solid Earth, v. 83, p. 1213–1226, https://doi.org/10.1029/JB083iB03p01213.
Kato, T., Beavan, J., Matsushima, T., Kotake, Y., Camacho, J.T., and Nakao, S., 2003, Geodetic evidence of backarc spreading in the Mariana Trough: Geophysical Research Letters, v. 30, no. 12, 1625, https://doi.org/10.1029/2002GL016757.
Key, K., Constable, S., Liu, L., and Pommier, A., 2013, Electrical image of passive mantle upwelling beneath the northern East Pacific Rise: Nature, v. 495, p. 499–502, https://doi.org/10.1038/nature11932.
Kitada, K., Seama, N., Yamazaki, T., Nogi, Y., and Suyehiro, K., 2006, Distinct regional differences in crustal thickness along the axis of the Mariana Trough, inferred from gravity anomalies: Geochemistry Geophysics Geosystems, v. 7, Q04011, https://doi.org/10.1029/2005GC001119.
Kong, L.S.L., 1993, Seafloor spreading in the Mariana Trough, *in* Segawa, J., ed., Preliminary Report of the Hakuho-Maru Cruise KH92–1: Tokyo, Japan, Ocean Research Institute, University of Tokyo, p. 5–16.
Kuo, B.-Y., and Forsyth, D.W., 1988, Gravity anomalies of the ridge-transform system in the South Atlantic between 31 and 34.5°S: Upwelling centers and variations in crustal thickness: Marine Geophysical Researches, v. 10, no. 3–4, p. 205–232, https://doi.org/10.1007/BF00310065.
Livermore, R., Cunningham, A., Vanneste, L., and Larter, R., 1997, Subduction influence on magma supply at the East Scotia Ridge: Earth and Planetary Science Letters, v. 150, p. 261–275, https://doi.org/10.1016/S0012-821X(97)00074-5.
Ma, L.Y., and Cochran, J.R., 1997, Bathymetric roughness of the Southeast Indian Ridge: Implications for crustal accretion at intermediate spreading rate mid-ocean ridges: Journal of Geophysical Research–Solid Earth, v. 102, p. 17697–17711, https://doi.org/10.1029/97JB01280.
Ma, Y., and Cochran, J.R., 1996, Transitions in axial morphology along the Southeast Indian Ridge: Journal of Geophysical Research–Solid Earth, v. 101, p. 15849–15866, https://doi.org/10.1029/95JB03038.
Macdonald, K.C., 1982, Mid-ocean ridges: Fine scale tectonic, volcanic and hydrothermal processes within the plate boundary zone: Annual Review of Earth and Planetary Sciences, v. 10, p. 155–190, https://doi.org/10.1146/annurev.ea.10.050182.001103.
Martinez, F., and Taylor, B., 2002, Mantle wedge control on backarc crustal accretion: Nature, v. 416, p. 417–420, https://doi.org/10.1038/416417a.
Martinez, F., and Taylor, B., 2003, Controls on back-arc crustal accretion: Insights from the Lau, Manus, and Mariana basins, *in* Larter, R.D., and Leat, P.T., eds., Intra-Oceanic Subduction Systems: Tectonic and Magmatic Processes: Geological Society [London] Special Publication 219, p. 19–54, https://doi.org/10.1144/GSL.SP.2003.219.01.02.
Martinez, F., and Taylor, B., 2006, Modes of crustal accretion in back arc basins: Inferences from the Lau Basin, *in* Christie, D.M., et al., eds., Back Arc Spreading Systems: Geological, Biological, Chemical, and Physical Interactions: American Geophysical Union Geophysical Monograph 166, p. 5–30, https://doi.org/10.1029/166GM03.
Martinez, F., Fryer, P., Baker, N., and Yamazaki, T., 1995, Evolution of backarc rifting: Mariana Trough, 20°N–24°N: Journal of Geophysical Research, v. 100, p. 3807–3827, https://doi.org/10.1029/94JB02466.
Martinez, F., Fryer, P., and Becker, N.C., 2000, Geophysical characteristics of the southern Mariana Trough, 11°50′N–13°40′N: Journal of Geophysical Research, v. 105, p. 16591–16607, https://doi.org/10.1029/2000JB900117.
Martinez, F., Okino, K., Ohara, Y., Reysenbach, A.-L., and Goffredi, S.K., 2007, Back-arc basins: Oceanography (Washington, D.C.), v. 20, no. 1, p. 116–127, https://doi.org/10.5670/oceanog.2007.85.
Martinez, F., Kelley, K.A., and Stern, R.J., 2012, Creation and deformation of hydrous lithosphere at the southern Mariana margin: Abstract EGU2012–6643, presented at 2012 European Geosciences Union General Assembly, EGU, Vienna, Austria, 22–27 April.
Martinez, F., Stern, R.J., Kelley, K.A., Ohara, Y., Sleeper, J.D., Ribeiro, J.M., and Brounce, M., 2018, Diffuse extension of the southern Mariana margin: Journal of Geophysical Research–Solid Earth, v. 123, p. 892–916, https://doi.org/10.1002/2017JB014684.
Masuda, H., 2006, Kairei Cruise KR06–11 Cruise Report, 1st–11th September, 2006, at Southern Mariana Trough: Japan Agency for Marine-Earth Science and Technology, JAMSTEC DARWIN archive, 46 p., https://doi.org/10.17596/0001060.
Masuda, H., and Fryer, P., 2015, Geochemical characteristics of active backarc basin volcanism at the southern end of the Mariana Trough, *in* Ishibashi, J.-i., Okino, K., and Sunamura, M., eds., Subseafloor Biosphere Linked to Hydrothermal Systems: Tokyo, Japan, Springer, p. 261–273, https://doi.org/10.1007/978-4-431-54865-2_21.
Mei, S., and Kohlstedt, D.L., 2000a, Influence of water on plastic deformation of olivine aggregates: 1. Diffusion creep regime: Journal of Geophysical Research–Solid Earth, v. 105, no. B9, p. 21457–21469, https://doi.org/10.1029/2000JB900179.
Mei, S., and Kohlstedt, D.L., 2000b, Influence of water on plastic deformation of olivine aggregates: 2. Dislocation creep regime: Journal of Geophysical Research–Solid Earth, v. 105, p. 21471–21481, https://doi.org/10.1029/2000JB900180.
Oakley, A.J., Taylor, B., Moore, G.F., and Goodliffe, A., 2009, Sedimentary, volcanic, and tectonic processes of the central Mariana Arc: Mariana Trough backarc basin formation and the West Mariana Ridge: Geochemistry Geophysics Geosystems, v. 10, Q08X07, https://doi.org/10.1029/2008GC002312.
Ohara, Y., Martinez, F., Brounce, M.N., Pujana, I., Ishii, T., Stern, R.J., Ribeiro, J., Michibayashi, K., Kelley, K.A., Reagan, M.K., Watanabe, H., Okumura, T., Oya, S., and Mizuno, T., 2014, The first *Shinkai* dive study of the southwestern Mariana arc system: San Francisco, California, American Geophysical Union, Fall Meeting, abstract T53A–4651.
Okino, K.Y., Shimakawa, Y., and Nagaoka, S., 1994, Evolution of the Shikoku Basin: Journal of Geomagnetism and Geoelectricity, v. 46, p. 463–479, https://doi.org/10.5636/jgg.46.463.
Okino, K.Y., Kasuga, S., and Ohara, Y., 1998, A new scenario of the Parece Vela Basin genesis: Marine Geophysical Researches, v. 20, p. 21–40, https://doi.org/10.1023/A:1004377422118.
Parker, R.L., 1972, The rapid calculation of potential anomalies: Geophysical Journal of the Royal Astronomical Society, v. 31, p. 447–455, https://doi.org/10.1111/j.1365-246X.1973.tb06513.x.
Parson, L.M., and Hawkins, J.W., 1994, Two-stage propagation and the geological history of the Lau backarc basin, *in* Hawkins, J.W., et al., eds., Proceedings of the Ocean Drilling Program, Scientific Results, Volume 135: College Station, Texas, Ocean Drilling Program, p. 819–828.
Parson, L.M., and Wright, I.C., 1996, The Lau-Havre-Taupo back-arc basin: A southward-propagating, multi-stage evolution from rifting to spreading: Tectonophysics, v. 263, p. 1–22, https://doi.org/10.1016/S0040-1951(96)00029-7.
Parsons, B., and Sclater, J.G., 1977, An analysis of the variation of ocean floor bathymetry and heat flow with age: Journal of Geophysical Research–Solid Earth, v. 82, p. 803–827, https://doi.org/10.1029/JB082i005p00803.
Peacock, S.A., 1990, Fluid processes in subduction zones: Science, v. 248, no. 4953, p. 329–337, https://doi.org/10.1126/science.248.4953.329.
Pearce, J.A., Stern, R.J., Bloomer, S., and Fryer, P., 2005, Geochemical mapping of the Mariana arc-basin system: Implications for the nature and distribution of subduction components: Geochemistry Geophysics Geosystems, v. 6, Q07006, https://doi.org/10.1029/2004GC000895.
Phipps Morgan, J., 1997, The generation of a compositional lithosphere by mid-ocean ridge melting and its effect on subsequent off-axis hotspot upwelling and melting: Earth and Planetary Science Letters, v. 146, p. 213–232, https://doi.org/10.1016/S0012-821X(96)00207-5.
Phipps Morgan, J., and Chen, Y.J., 1993, Dependence of ridge-axis morphology on magma supply and spreading rate: Nature, v. 364, no. 6439, p. 706–708, https://doi.org/10.1038/364706a0.
Reagan, M.K., Heywood, L., Goff, K., Michibayashi, K., Foster, C.T., Jr., Jicha, B., Lapen, T., McClelland, W.C., Ohara, Y., Righter, M., Scott, S., and Sims, K.W.W., 2018, Geodynamic implications of crustal lithologies from the southeast Mariana forearc: Geosphere, v. 14, no. 1, p. 1–22, https://doi.org/10.1130/GES01536.1.
Resing, J.A., Rubin, K.H., Embley, R.W., Lupton, J.E., Baker, E.T., Dziak, R.P., Baumberger, T., Lilley, M.D., Huber, J.A., Shank, T.M., Butterfield, D.A., Clague, D.A., Keller, N.S., Merle, S.G., Buck, N.J, Michael, P.J., Soule, A., Caress, D.W., Walker, S.L., and Davis, R., 2011, Active submarine

eruption of boninite at West Mata volcano in the extensional NE Lau Basin: Nature Geoscience, v. 4, p. 799–806, https://doi.org/10.1038/ngeo1275.

Ribeiro, J.M., Stern, R.J., Martinez, F., Ishizuka, O., Merle, S.G., Kelley, K.A., Anthony, E.Y., Ren, M., Ohara, Y., Reagan, M., Girard, G., and Bloomer, S., 2013, Geodynamic evolution of a forearc rift in the southernmost Mariana Arc: The Island Arc, v. 22, p. 453–476, https://doi.org/10.1111/iar.12039.

Ribeiro, J.M., Stern, R.J., Kelley, K.A., Shaw, A.M., Martinez, F., and Ohara, Y., 2015, Composition of the slab-derived fluids released beneath the Mariana forearc: Evidence for shallow dehydration of the subducting plate: Earth and Planetary Science Letters, v. 418, p. 136–148, https://doi.org/10.1016/j.epsl.2015.02.018.

Rognstad, M.R., 1992, HAWAII MR1: A new underwater mapping tool, paper presented at International Conference on Signal Processing and Technology: Honolulu, Hawaii, PACON International, November 1992, p. 900–905.

Rognstad, M.R., 2005, The IMI-30: A 30 kHz imaging and mapping instrument: Proceedings of OCEANS 2005 MTS/IEEE, v. 3, p. 2742–2745, https://doi.org/10.1109/OCEANS.2005.1640188.

Sandwell, D.T., Muller, R.D., Smith, W.H.F., Garcia, E., and Francis, R., 2014, New global marine gravity model from CryoSat-2 and Jason-1 reveals buried tectonic structure: Science, v. 346, no. 6205, p. 65–67, https://doi.org/10.1126/science.1258213.

Sato, T., Mizuno, M., Takata, H., Yamada, T., Isse, T., Mochizuki, K., Shinohara, M., and Seama, N., 2015, Seismic structure and seismicity in the southern Mariana Trough and their relation to hydrothermal activity, *in* Ishibashi, J.-i., Okino, K., and Sunamura, M., eds., Subseafloor Biosphere Linked to Hydrothermal Systems: Tokyo, Japan, Springer, p. 229–240, https://doi.org/10.1007/978-4-431-54865-2_18.

Schmidt, M.W., and Poli, S., 1998, Experimentally based water budgets for dehydrating slabs and consequences for arc magma generation: Earth and Planetary Science Letters, v. 163, p. 361–379, https://doi.org/10.1016/S0012-821X(98)00142-3.

Scordilis, E.M., 2006, Empirical relations converting $M_S$ and $m_b$ to moment magnitude: Journal of Seismology, v. 10, p. 225–236, https://doi.org/10.1007/s10950-006-9012-4.

Scott, R., and Kroenke, L., 1980, Evolution of back arc spreading and arc volcanism in the Philippine Sea: Interpretation of Leg 59 DSDP results, *in* Hayes, D.E., ed., The Tectonic and Geologic Evolution of Southeast Asian Seas and Islands: American Geophysical Union Geophysical Monograph 23, p. 283–291, https://doi.org/10.1029/GM023p0283.

Scott, R., and Kroenke, L., 1981, Periodicity of remnant arcs and back-arc basins of the South Philippine Sea, *in* von Huene, R., ed., Oceanologica Acta, Proceedings of the 26th International Geological Congress, Geology of Continental Margins Symposium, Paris, 7–17 July 1980, p. 193–202.

Seama, N., and Fujiwara, T., 1993, Geomagnetic anomalies in the Mariana Trough, 18°N, *in* Segawa, J., ed., Preliminary Report of the Hakuho-Maru Cruise KH92–1: Tokyo, Japan, Ocean Research Institute, University of Tokyo, p. 70–73.

Seama, N., and Okino, K., 2015, Asymmetric seafloor spreading of the southern Mariana Trough backarc basin, *in* Ishibashi, J.-i., Okino, K., and Sunamura, M., eds., Subseafloor Biosphere Linked to Hydrothermal Systems: Tokyo, Japan, Springer, p. 253–260, https://doi.org/10.1007/978-4-43154865–2_20.

Seno, T., Stein, S., and Gripp, A.E., 1993, A model for the motion of the Philippine Sea plate consistent with NUVEL-1 and geological data: Journal of Geophysical Research–Solid Earth, v. 98, no. B10, p. 17941–17948, https://doi.org/10.1029/93JB00782.

Sleeper, J.D., and Martinez, F., 2014, Controls on segmentation and morphology along the back-arc Eastern Lau spreading center and Valu Fa Ridge: Journal of Geophysical Research–Solid Earth, v. 119, p. 1678–1700, https://doi.org/10.1002/2013JB010545.

Sleeper, J.D., and Martinez, F., 2016, Geology and kinematics of the Niuafo'ou microplate in the northern Lau Basin: Journal of Geophysical Research–Solid Earth, v. 121, p. 4852–4875, https://doi.org/10.1002/2016JB013051.

Sleeper, J.D., Martinez, F., and Arculus, R., 2016, The Fonualei Rift and spreading center: Effects of ultraslow spreading and arc proximity on axial morphology: Journal of Geophysical Research–Solid Earth, v. 121, p. 4814–4835, https://doi.org/10.1002/2016JB013050.

Smith, W.H.F., and Sandwell, D.T., 1997, Global seafloor topography from satellite altimetry and ship depth soundings: Science, v. 277, p. 1956–1962, https://doi.org/10.1126/science.277.5334.1956.

Solomon, S.C., Huang, P.Y., and Meinke, L., 1988, The seismic moment budget of slowly spreading ridges: Nature, v. 334, p. 58–60, https://doi.org/10.1038/334058a0.

Spiegelman, M., and McKenzie, D., 1987, Simple 2-D models for melt extraction at mid-ocean ridges and island arcs: Earth and Planetary Science Letters, v. 83, p. 137–152, https://doi.org/10.1016/0012-821X(87)90057-4.

Stern, R.J., and Smoot, N.C., 1998, A bathymetric overview of the Mariana forearc: The Island Arc, v. 7, no. 3, p. 525–540, https://doi.org/10.1111/j.1440-1738.1998.00208.x.

Stern, R.J., Smoot, N.C., and Rubin, M., 1984, Unzipping of the Volcano Arc, Japan: Tectonophysics, v. 102, p. 153–174, https://doi.org/10.1016/0040-1951(84)90012-X.

Stern, R.J., Fouch, M.J., and Klemperer, S.L., 2004, An overview of the Izu-Bonin-Mariana subduction factory, *in* Eiler, J., ed., Inside the Subduction Factory: American Geophysical Union Geophysical Monograph 138, p. 175–222, https://doi.org/10.1029/138gm10.

Stern, R.J., Tamura, Y., Masuda, H., Fryer, P., Martinez, F., Ishizuka, O., and Bloomer, S.H., 2013, How the Mariana volcanic arc ends in the south: The Island Arc, v. 22, p. 133–148, https://doi.org/10.1111/iar.12008.

Stern, R.J., Ren, M., Kelley, K.A., Ohara, Y., Martinez, F., and Bloomer, S.H., 2014, Basaltic volcaniclastics from the Challenger Deep forearc segment, Mariana convergent margin: Implications for tectonics and magmatism of the southernmost Izu-Bonin-Mariana arc: The Island Arc, v. 23, no. 4, p. 368–382, https://doi.org/10.1111/iar.12088.

Stern, R.J., Ohara, Y., Ren, M., Leybourne, M., and Bowers, B., 2020, Glimpses of oceanic lithosphere of the Challenger Deep forearc segment in the southernmost Marianas: The 143°E transect, 5800–4200 m: The Island Arc, v. 29, no. 1, p. e12359, https://doi.org/10.1111/iar.12359.

Stolper, E., and Newman, S., 1994, The role of water in the petrogenesis of Mariana Trough magmas: Earth and Planetary Science Letters, v. 121, p. 293–325, https://doi.org/10.1016/0012-821X(94)90074-4.

Taylor, B., and Martinez, F., 2003, Backarc basin basalt systematics: Earth and Planetary Science Letters, v. 210, p. 481–497, https://doi.org/10.1016/S0012-821X(03)00167-5.

Taylor, B., Goodliffe, A.M., and Martinez, F., 1999, How continents break up: Insights from Papua New Guinea: Journal of Geophysical Research, v. 104, p. 7497–7512, https://doi.org/10.1029/1998JB900115.

Wan, K., Lin, J., Xia, S., Sun, J., Xu, M., Yang, H., Zhou, Z., Zeng, X., Cao, J., and Xu, H., 2019, Deep seismic structure across the southernmost Mariana Trench: Implications for arc rifting and plate hydration: Journal of Geophysical Research–Solid Earth, v. 124, p. 4710–4727, https://doi.org/10.1029/2018JB017080.

Watanabe, M., Okino, K., and Kodera, T., 2010, Rifting to spreading in the southern Lau Basin: Variations within the transition zone: Tectonophysics, v. 494, no. 3–4, p. 226–234, https://doi.org/10.1016/j.tecto.2010.09.001.

Watts, A.B., and Talwani, M., 1975, Gravity effect of downgoing lithospheric slabs beneath island arcs: Geological Society of America Bulletin, v. 86, p. 1–4, https://doi.org/10.1130/0016-7606(1975)86<1:GEODLS>2.0.CO;2.

Wessel, P., Luis, J.F., Uieda, L., Scharroo, R., Wobbe, F., Smith, W.H.F., and Tian, D., 2019, The Generic Mapping Tools version 6: Geochemistry Geophysics Geosystems, v. 20, p. 5556–5564, https://doi.org/10.1029/2019GC008515.

Wysoczanski, R.J., Todd, E., Wright, I.C., Leybourne, M.I., Hergt, J.M., Adam, C., and Mackay, K., 2010, Backarc rifting, constructional volcanism, and nascent disorganized spreading in the southern Havre Trough backarc rifts (SW Pacific): Journal of Volcanology and Geothermal Research, v. 190, p. 39–57, https://doi.org/10.1016/j.jvolgeores.2009.04.004.

Yamazaki, T., Seama, N., Okino, K., Kitada, K., Joshima, M., Oda, H., and Naka, J., 2003, Spreading process of the northern Mariana Trough: Rifting-spreading transition at 22°N: Geochemistry Geophysics Geosystems, v. 4, no. 9, 1075, https://doi.org/10.1029/2002GC000492.

Zhu, G., Yang, H., Lin, J., Zhou, Z., Xu, M., Sun, J., and Wan, K., 2019, Along-strike variation in slab geometry at the southern Mariana subduction zone revealed by seismicity through ocean bottom seismic experiments: Geophysical Journal International, v. 218, no. 3, p. 2122–2135, https://doi.org/10.1093/gji/ggz272.